UNIVERSITY OF CALIFORNIA

Santa Barbara

Best Methods for Obtaining Absolute Water Velocity Profiles from Gliders with ADCPs

A thesis submitted in partial satisfaction of the

requirements for the degree Master of Science

in Marine Science

by

Daniel Painter Ellis

Committee in charge:

Professor Libe Washburn, Chair

Dr. Carter Ohlmann

Professor Tommy Dickey

March 2016

The thesis of Daniel Painter Ellis is approved by:

_____

Carter Ohlmann

_____

Tommy Dickey

_____

Libe Washburn, Committee Chair

March 2016

Best Methods for Obtaining Absolute Water Velocity Profiles from Gliders with ADCPs

ACKNOWLEDGMENTS

I will start with my committee members without whom this paper would still have been possible, but a lot more work for them. I will also thank Chris Gotschalk. I will then thank Chris again. And again. His help with Matlab and data processing were instrumental to this paper and he was an invaluable asset throughout my time at UCSB. Finally, my family and girlfriend who, even in the face of severe adversity, encouraged me to keep going.

Best Methods for Obtaining Absolute Water Velocity Profiles from Gliders with ADCPs

Daniel P. Ellis, Carter Ohlmann, Libe Washburn, Oscar Schofield, and Mark Moline

Abstract

Autonomous underwater vehicles (AUVs) like gliders are typically used to obtain vertical cross sections of water properties along transects. Another, less common, application is the use of gliders as virtual moorings. Gliders offer many advantages compared with conventional moorings, but extensive evaluation of gliders as mooring substitutes has not been done. Here, temperature and ocean current velocity data from coincidently deployed gliders-as- moorings and moorings are compared to assess the fidelity of glider-as-mooring data. The glider-as-mooring data were processed in a variety of ways and compared with mooring. During August 2012, two gliders sampled in a box pattern around a conventional mooring in 26 m water depth off of Pt. Sal, California for two and six days, respectively. Two box patterns were used, one 500 m on a side (two and four days) and the other 1 km on a side (two days). Temperature and velocity data from the gliders and moorings are compared using linear regressions and contouring techniques. Linear regressions show good agreement between glider and mooring temperatures ($r^2 = 0.89$, $p < 0.001$). Significant correlations are also found between ADCP-derived velocities from the gliders and the mooring; along-shore velocities exhibit higher correlation ($r^2 = 0.70$, $p < 0.001$) compared with cross-shore velocities ($r^2 = 0.37$, $p < 0.001$). Glider versus glider comparisons are similar to glider versus mooring comparisons in the along-shore ($r^2 = 0.60$, $p < 0.001$) and cross-shore ($r^2 = 0.36$, $p < 0.001$) directions. Temperature comparisons between gliders also show good agreement ($r^2 = 0.93$, $p < 0.001$).

1) Introduction

Autonomous Underwater Vehicles (AUVs) were developed as an economical alternative to ship-based sampling that requires significant labor and fuel costs. AUVs now routinely collect data along transects. These transects vary in length from several thousand km (width of the pacific ocean) to less than 1 km. Relatively expensive ship operations are still a part of deployment and retrieval of moorings. In a further effort to develop economical alternatives to ship-based operations, this study examines the use of AUVs as moorings. Ocean gliders are an ideal tool for observing coastal ocean phenomenon due to their ability to sample the water column with high temporal resolution and transmit data to shore in near real-time. By using buoyancy propulsion to control vertical position and wings to generate forward motion (Davis et al., 2003), gliders can move from waypoint to waypoint collecting vertical profiles during each upcast and downcast. In addition to using gliders for longer, repeated horizontal transects, (e.g. Eriksen et al., 2001; Davis, 2008) gliders can be used as virtual moorings (Sherman et al., 2001; Chiodi and Eriksen, 2002). One sampling mode for gliders acting as virtual moorings is to—as best they can—keep station while collecting vertical profiles (Rudnick et al., 2004). Although the forward motion of the glider and horizontal advection by currents prevent the glider from maintaining its exact position, gliders can maintain horizontal position as well as a surface buoy on the order of 1 km (Weller et al., 1990).

Previous studies using gliders as virtual moorings have sampled physical phenomena (Sherman et al., 2001) as well as biological phenomena like phytoplankton layers and DCM (Hodges and Fratantoni, 2009). Gliders in both studies were programmed collect vertical profiles at a single geographic position instead of performing transects. This mode of

virtually mooring gliders is referred to as keeping station since the glider is attempting to maintain its horizontal position. Sherman et al. (2001) used a spray glider in the Monterey Bay underwater canyon to keep station in 380 m water depth and collect temperature and conductivity profiles. The glider maintained its position within about 2.5 km for 11 days (see figure 5 of Sherman et al., 2001) and provided data about the effects of canyon bathymetry on internal tides. Hodges and Fratantoni (2009) used a "synthetic moored array" of five gliders profiling to 200 m water depth to sample a 100 km^2 area. The gliders used by Hodges and Fratantoni (2009) collected data from CTDs, fluorometers, backscatter sensors, and PAR modules in order to determine the spatial and temporal structure of chlorophyll in the Philippine Sea. All four of these gliders maintained an RMS distance from the desired location of less than 4 km (Hodges and Fratantoni 2009).

Gliders programmed to keep station provide information about the entire water column but, like moorings, do not provide details about the surrounding waters that can vary on small spatial scales (Ohlmann et al 2012). Rather than have gliders keep station, an alternative method is to have them orbit a point of interest in a box-like pattern (Fratantoni and Lund 2006; Mahoney et al., 2009). Using gliders, therefore, to sample in a box pattern combines the advantages of both methods—longer transects and station-keeping point measurements. Pettigrew et al (2014) deployed a Slocum G2 glider within 5km of a University of Maine buoy with a mounted ADCP and observed tidal flow in the glider data similar to results from the mooring, though a quantitative analysis of glider and mooring data was not done.

To our knowledge, this study is the first to compare data sets from gliders acting as virtually moorings gliders and existing moorings in the same location. This study examines

two box patterns of different sizes, 1 km and 500 m per side centered around a mooring with a bottom-mounted ADCP and a vertical array of temperature sensors. We aim to get a more quantitative understanding of glider as mooring data of scalar variables such as temperature, and include a specific focus on current profiles not addressed in past studies. The study also examines data-processing techniques for glider-mounted ADCPs and determination of angle of attack for these gliders.

For gliders operating with downward-looking ADCPs, bottom tracking can be used to obtain platform velocities but errors of order 5 cm s^{-1} can still occur (Fong and Monismith, 2004). If bottom tracking is unavailable, other methods must be used. One alternate method of obtaining current velocity from gliders is the "shear method". Ordonez et al., (2012) calculate a shear value from raw velocity measurements for each depth bin over a dive.

We evaluate three methods for estimating vertically averaged currents from gliders that in turn are used to estimate depth-resolved currents. In this paper, we use the methods developed by Todd et al. (2011) and Visbeck (2002) to estimate depth-resolved currents from gliders with externally mounted, upward-looking ADCPs. This method requires estimating the horizontal velocity of the glider through the water to then calculate vertically averaged currents. We compare vertically averaged currents obtained using three methods to derive the horizontal velocity of the gliders through the water with data from the bottom-mounted ADCP that provides independent estimates of vertically averaged currents. We also compare depth-resolved currents from the gliders with depth-resolved currents from the bottom-mounted ADCP.

The methods used in this work are presented in section 2, including a description of contouring and regression techniques for each variable. Section 3 shows glider versus mooring velocity and mooring temperature as well as glider versus glider comparisons for velocity and temperature. Section 4 discusses the results and suggests future research and applications for gliders and data processing techniques. A notable increase in correlation of temperature and velocity data between the glider and mooring was observed for the 500 m box compared to the 1 km box. We also found that using the glider's pitch and vertical velocity provided the best agreement in vertically averaged velocity with the mooring when a correction to angle of attack was applied.

2) Methods

2.1) Field Site

The field site is located on the continental shelf off the central California coast, just north of Point Conception. Point Conception is an important biogeographic boundary between the north-south oriented Central California coast and the more East-West oriented Southern California Bight. North of Point Conception the ocean circulation is primarily an upwelling regime characterized by relatively cool water and equatorward currents. South of Point Conception, the coastal circulation is often characterized by poleward coastal flows and much warmer waters associated with the Southern Californian Bight circulation. Characteristic patterns of ocean circulation in the study region, along with wind and water property information are well documented in studies by Hickey (1979), and Winant et al. (2003).

The field site at Point Sal was selected in an effort to understand the intermittent poleward flow of Southern California bight waters north of Point Conception along the California Coast (Melton et al. 2009). The site is located more than 30 km from the nearest port in relatively rough waters. This makes access by small boat relatively difficult. Larger vessels that can handle the distance from port and relatively rough conditions could be used, but are economically prohibitive. Therefore, moorings and gliders were selected as the primary sampling platforms for the project.

2.2) Mooring instrumentation

The mooring was instrumented with: a Sea Bird Electronics SBE39 temperature and pressure sensor with a resolution of 0.002 °C and 0.05 dbar respectively, located 20.4 m above the bottom; Onset Computer Corporation temperature tidbits with ± 0.024 °C accuracy, located 17.1, 11.6, 6.7, and 1.2 m above the bottom; a Sea Bird Electronics SBE26plus wave, tide, and temperature recorder with resolution of 0.02 dbar and temperature resolution of 0.001 °C; and an upward looking Teledyne RD Instruments 614.4 kHz Workhorse Sentinel ADCP with a resolution of 0.1 cm s^{-1} ± 1.17 cm s^{-1}, and a blanking distance of 0.88 m. Both the SBE26plus and ADC were located at the mooring base on the seafloor. Temperature measurements made by all the instruments on the mooring are recorded every 4 minutes. Pressure data from the SBE26plus are averaged for 2 minute intervals and recorded every 4 minutes. The bottom-mounted ADCP (subsequently referred to as moored ADCP) used a ping interval of 1.5 Hz with 36 pings per ensemble at an ensemble interval of 150 seconds meaning each vertical profile of currents is averaged over a 54 second interval with 96 seconds of idle time between measurements. These data are averaged into 1 m bins and the top two bins are omitted due to side-lobe effects and surface

waves (van Haren, 2001). The instrumentation on the mooring was selected to capture the changes in vertical water properties and horizontal currents associated with poleward flows. The mooring was constructed at UCSB and deployed with a small (< 30 ft) boat.

2.3) Glider instrumentation

The three gliders used in the study are Teledyne Webb Research (TWR) Coastal G1 gliders equipped with a Sea Bird Electronics SBE41 pumped CTD that sampled at 0.5 Hz. Gliders are also equipped with externally-mounted 1 MHz Nortek Aquadopp Profilers that sampled at 0.5 - 1 Hz. Each ADCP (subsequently referred to as glider ADCP) is mounted so its beams are oriented vertically upward during glider descent.

Gliders were launched from Port San Luis, CA, located roughly 33 km north of the study site (Figure 1). Gliders were programmed to fly to the mooring location (roughly three days travel time), fly box-patterns around the mooring (Figure1b), and return to Port San Luis. Glider RU06 (glider 6 in the Rutgers University glider fleet) arrived at the mooring on 6 August 2012, flew a counter-clockwise box pattern of 1 km per side for two days, then switched to a 500 m per side counter-clockwise box pattern for four days. Glider RU05 arrived at the mooring on 10 August 2012 and flew a clockwise box pattern with 500 m per side for two days. In 2013, both RU05 and RU07 arrived at the mooring on 17 August and sampled clockwise and counter-clockwise 500 m per side box patterns, respectively, for two days. The two different box sizes were selected to examine how increases in spatial averaging influence a gliders' ability to represent moored instrument observations. The time each glider flew a box pattern was constrained by battery life and other goals (flight patterns) of the glider mission.

Glider ADCPs sampled ten 1 m bins beginning 0.2 to 0.4 m above the instrument (i.e. blanking distance). Raw current velocities measured with the glider ADCP are relative to the glider motion, and subsequently identified as $\mathbf{u}(z,t)_{rel}$, where t and z are time and vertical coordinate, respectively. Bold variables throughout indicate vector quantities with components in the eastward and northward directions. Determining absolute ocean current velocity from glider ADCP requires summing the glider velocity relative to the Earth and the water velocity relative to the moving glider.

2.4) Data Processing

2.4.1) Temperature and Velocity Comparisons

The vertical coordinate system used in this study is defined as height above bottom (HAB) at the location of the mooring. Changes in depth of the water column can vary on the order of 1 – 2 m day^{-1} primarily due to barotropic tidal fluctuations. These variations are observed with the moored pressure sensors. The HAB coordinate system allows the vertical position of glider observations to be easily aligned with moored observations throughout a tidal cycle. Glider HAB $h_g(t)$, at time t is computed as

$$h_g(t)=h_w(t)-d_g(t) \quad \text{Eq. (1)}$$

where $h_w(t)$ is the time dependent total water column height measured by the moored bottom pressure sensor and $d_g(t)$ is the depth of the glider below the sea surface measured by its CTD. Strictly speaking, HAB is not the exact time dependent distance between the

(horizontally moving) glider and the sea-floor; but rather a convenient coordinate system defined at the mooring location. Linear interpolation of $h_w(t)$ is used to determine total water column height at the exact sampling times of the glider CTD.

When comparing glider and mooring temperature data, the measurements are required to be recorded within ± 1 minute and between ± 0.25 m in the vertical. In the case of multiple glider temperature measurements meeting these criteria, temperatures are averaged over the time and height intervals encompassing the mooring measurement. On average, ~ 4 glider temperature measurements are averaged together for comparison with each mooring temperature. The time and vertical coordinate thresholds, subsequently referred to as the "search method," were chosen to maximize the coefficient of determination (r^2) between glider and mooring temperature observations.

An additional method of comparison is linear interpolation of glider temperatures to the HAB locations of the moored temperature sensors. Comparisons are then made between observations that are closest in time. This method is subsequently referred to as the "interpolation method".

Velocity comparisons between the moored and glider-mounted ADCP observations are initially performed with vertically averaged values and then with vertically dependent profiles. Vertically averaged currents from the moored ADCP are found for each time interval between glider surfacings. Velocity data included in the averaging are recorded every 2.5 minutes in 1 m bins from 3 m to 23 m above the bottom.

Vertically averaged currents from the glider between surfacings, $\mathbf{U}(t)$ are computed as the difference between the gliders actual position at subsequent surfacing determined by

GPS, $\mathbf{X}_{GPS}(t)$, and its "dead-reckoned" position at the surfacing, $\mathbf{X}_{DR}(t)$, divided by the flight time to the subsequent surfacing, Δt, or

$$\mathbf{U}(t) = [\mathbf{X}_{GPS}(t) - \mathbf{X}_{DR}(t)]/\Delta t \qquad \text{Eq. (2)}$$

$\mathbf{X}_{DR}(t)$, further discussed in Section X.X, is the expected glider surfacing location computed by integrating the velocity of the glider through the water. The difference in "dead-reckoned" and actual surfacing locations is attributed to the "vertically average" current field that pushes the glider off its "dead-reckoned" track. $\mathbf{U}(t)$ is defined to be at the midpoint in time between the two subsequent glider surfacings determined by GPS.

Vertically-resolved velocity profiles relative to glider motion are computed from the raw glider ADCP data, $\mathbf{u}(t,z)_{rel}$, following methods given by Visbeck (2002) and Todd et al (2011). Average vertically resolved velocity profiles relative to glider motion with a zero mean, $\mathbf{u}'(t,x)$ are computed at the mean time and position between glider surfacings by averaging glider ADCP profiles during all glider downcasts between glider surfacings using

$$\mathbf{u}'(z,t) = (G^T * G)^{-1} * G^T * \mathbf{u}(z,t)_{rel}$$

Eq. (3)

where G is the matrix of known and unknown ocean velocity measurements (see Visbeck (2002) and Todd et al (2001) for a rigorous explanation) obtained from the glider ADCP. Absolute, height-resolved velocity from the glider ADCP, $\mathbf{u}(z,t)$, is then computed at each

midpoint between glider surfacings as the sum of the vertically averaged (Equation 2) and vertically resolved (Equation 3) velocities or

$$\mathbf{u}(z,t) = \mathbf{U}(t) + \mathbf{u}'(z,t)$$

Eq. (4)

Only ADCP data from the ascending component of glider tracks are used in calculation of **u'**(z,t) (equation 3) due to the orientation of the beams relative to the vertical. The moored ADCP directly measures **u**(z,t). **U**(t) from the moored ADCP observations is calculated by averaging over times between glider surfacings (time of initial descent after data transmission to time of next surfacing for the subsequent data transmission). Finally **u**'(z,t) from the mooring is computed following Equation 4 by averaging **u**(z,t) profiles between glider surfacings and subtracting **U**(t).

2.4.2) Angle of Attack

Since the glider ADCP is measuring water velocity relative to the moving glider, obtaining accurate ocean current velocities from glider-mounted ADCPs requires knowledge of the glider velocity relative to the earth. This ultimately depends on the accuracy of $X_{DR}(t)$ (Equation 2). $X_{DR}(t)$ can be computed in a variety of ways (Section X.X.X), all of which require glider angle of attack to be known.

Glider angle of attack, α, is defined to be the angle between the glider's long axis and the path the glider takes through the water. α is a function of glider drag, lift, vertical velocity, and pitch. The glider's internal algorithms set α = 0° to simplify equations and thus

reduce computational time/energy. However, α is not strictly 0°, especially considering added drag associated with the externally mounted ADCP used in this study.

Here, α is determined by maximizing the value of r^2 between vertically-averaged currents from the glider and the moored ADCPs. α is found to be 3.7° and 3.4° for gliders RU06 and RU05, respectively. These values are the values used in the various dead-reckoning position calculations presented in the next section

2.4.3) Dead-reckoned glider position

Three methods are used to compute the glider's velocity through the water, and thus the dead-reckoned glider position ($\mathbf{X}_{DR}(t)$; Equation 2). The three methods are subsequently referred to as "glider," "beam," and "enu"; with their resulting velocities referred to as $\mathbf{u}_{G,DR,glider}(t)$ $\mathbf{u}_{G,DR,beam}(t)$, and $\mathbf{u}_{G,DR,enu}(t)$ respectively, and resulting dead-reckoned positions referred to as $\mathbf{X}_{DR,glider}(t)$, $\mathbf{X}_{DR,beam}(t)$, and $\mathbf{X}_{DR,enu}(t)$, respectively. $\mathbf{X}_{DR,<method>}(t)$, equivalent to $\mathbf{X}_{DR}(t)$ in Equation 2, is computed as the time integral of $\mathbf{u}_{G,DR,<method>}(t)$, where the subscripts indicate the velocity is that of the glider ("G") computed from a dead reckoned position ("DR") using one of three methods ("<method>"). The "glider" method uses flight characteristics of the glider, including its vertical velocity as measured with the glider's CTD. The "beam" method uses data from the two ADCP beams with components along the axis of glider travel. The "enu" method adds the vertically oriented ADCP beam.

The "glider" method depends on the gliders pitch, angle of attack, and vertical velocity, and is computed as.

$$\mathbf{u}_{G,DR,glider}(t) = (dp/dt)\tan(\theta(t) + \alpha))^{-1}$$

Eq. (5)

where dp/dt is the time derivative of pressure, θ(t) is glider pitch as measured by the glider internally and α is the calculated angle of attack.. $\mathbf{u}_{G,DR,glider}(t)$ is computed from the 0.5 Hz glider data, and $\mathbf{X}_{DR,glider}(t)$ is computed by integrating $\mathbf{u}_{G,DR,glider}(t)$ between glider surfacings.

The "beam" method uses water velocity relative to the moving glider as measured directly by beams 2 and 3 on the glider-mounted ADCP. Beams 2 and 3 point upward and rearward, respectively, and thus measure parallel to the long axis of the glider. Beam 1 is oriented perpendicularly to the glider's long axis. Thus, the long axis component of velocity is zero, and the beam can be ignored. The "beam" method then determines the long axis component of velocity as the average of velocities measured by beams 2 and 3, or

$$\mathbf{u}_{G,DR,beam}(t)= [(B_2(t) + B_3(t))/2] \cos(\beta)^{-1}\cos(\theta(t)) + \alpha)$$

Eq. (6)

where B_2 and B_3 are the along beam velocities measured by the glider ADCP with beams 2 and 3 respectively, β is the angle of beams 2 and 3 with respect to the glider's long axis, and θ is defined as in (5). For the ADCPs used here, β = 55° and B_2 and B_3 velocities are from the two bins nearest the ADCP. $\mathbf{u}_{G,DR,beam}(t)$ is computed from the 1.0 Hz ADCP data, and $\mathbf{X}_{DR,beam}(t)$ is computed by integrating $\mathbf{u}_{G,DR,gbeam}(t)$ between glider surfacings.

The “enu” method uses water velocity relative to the moving glider as measured by all three ADCP beams. In addition to using beam 3 data from the ADCP, the method uses a set of transformation matrices to convert the beam data into geophysical coordinates (east, north, and up; thus “enu”). The beam method computes the eastward, northward, and upward components of velocity as

$$\mathbf{u}_{G,DR,enu}(t) = R(t)\,[B_1(t)\ B_2(t)\ B_3(t)]^T$$

Eq. (7)

where B_1, B_2 and B_3 are the along beam velocities measured by the glider ADCP with beams 1, 2 and 3 respectively, and R(t) is the beam-to-geophysical coordinate transformation matrix defined as

$$R(t) = T*H(t)*P(t)$$

Eq. (8)

that depends on ADCP orientation and glider flight characteristics. In Equation 8, T is the transformation matrix obtained from the manufacturer

$$T = \begin{Bmatrix} -1.2744 & 0.8708 & 0.8708 \\ 0.00 & 1.3662 & -1.3662 \\ 1.000 & 0.000 & 0.000 \end{Bmatrix}$$

Eq. (9)

P is the “pitch” matrix that depends on measurements from the glider’s tilt sensors of pitch, roll, and angle of attack given as, $\theta(t)$, $\xi(t)$, and α, respectively

$$P(t) = \begin{Bmatrix} \cos(\theta(t)+\alpha) & -\sin(\theta(t)+\alpha)\sin(\xi(t)) & -\cos(\xi(t))\sin(\theta(t)+\alpha) \\ 0 & \cos(\xi(t)) & -\sin(\xi(t)) \\ \sin(\theta(t)+\alpha) & \sin(\xi(t))\cos(\theta(t)+\alpha) & \cos(\theta(t)+\alpha)\cos(\xi(t)) \end{Bmatrix} \quad \text{Eq. (10)}$$

and H is the heading matrix that depends on glider’s heading, $\phi(t)$ determined by the glider’s compass,

$$H(t) = \begin{Bmatrix} \cos(\phi(t)) & \sin(\phi(t)) & 0 \\ -\sin(\phi(t)) & \cos(\phi(t)) & 0 \\ 0 & 0 & 1 \end{Bmatrix} \quad \text{Eq. (11)}$$

$\mathbf{u}_{G,DRenu}(t)$ is computed from glider and ADCP data every 2 seconds, and $\mathbf{X}_{DR,enu}(t)$ is computed by integrating $\mathbf{u}_{G,DR,enu}(t)$ between glider surfacings. Both the beam and enu methods utilize ADCP data collected on both glider descents and ascents for determining $\mathbf{X}_{DR}(t)$ and thus $\mathbf{U}(t)$ (Equation 2).

3) Results

3.1) Temperature

Unlike moored temperature sensors, typically at a fixed height, gliders move vertically and thus only sample a specific height when moving through that height. In addition, gliders must suspend sampling while at the surface transferring data. The

distribution of time between glider T(z) samples depends on the sampling height (z), the maximum height over which the glider profiles (z_max; assuming the glider samples from the surface downward) and the time to transfer data. Heights sampled near the surface and bottom of glider profiles will have a short interval between samples, followed by a much longer interval. Heights sampled near the middle of the glider profile will experience more uniform times between samples collected on the glider downcast and subsequent upcast. The average time between T(z) samples depends on z_max and the time needed for data transfer, not necessarily z.

The average time between glider T(z) samples is 4.6 minutes (σ = 2.2 minutes) for z_max = 24 m, not considering breaks in sampling for data transfer when the glider spends extended time at the surface. For comparison, the moored T(z) measurements are taken every 4.0 minutes. Neither sampling times nor frequencies between the platforms are exactly aligned. For gliders sampling the 500 m box, the average underwater sampling time is 33.9 minutes (σ = 15.5 minutes) and the average time at the surface for data transfer is 9.2 minutes (σ = 2.2 minutes). For the glider sampling the 1 km box, where surfacing intervals are less frequent, the average underwater sampling time is 42.4 minutes (σ = 20.0 minutes) and the average time at the surface for data transfer is 13.7 minutes (σ = 29.5 minutes). Thus, glider profiling occurs 79 and 76% of the time the glider is in the water for the 500 m and 1 km boxes, respectively.

Despite differing sampling frequencies and locations, T(z) time-series from the two platforms show generally similar time varying patterns (Figure 2). However, times exist where T(z) differences between the platforms exceed 1 C, primarily at the shallowest (20.4 HAB) height. For example, early on 8/07/12 and 8/10/12, T(z) increases of roughly 1 °C

observed with gliders lag those recorded with the moored sensors by roughly 1 – 2 hours (Figure 2a). A multi-hour period exists early on 8/18/13 where T(z) observed with gliders is roughly 1 C cooler than T(z) measured with moored sensors (Figure 2d). These differences between measurement platforms are presumably due to small-scale variations in the horizontal and/or vertical temperature distributions, combined with the discrepancy in sampling times/locations between platforms. Differences in sampling locations range from roughly 250 to 360, and 500 to 710 m for the 500 m and 1 km sampling boxes, respectively (Figure 1b).

Although instantaneous differences are expected to exist between platforms, T(z) statistics should be in close agreement if gliders are to be used as virtual moorings. Mean T(z) differences between the mooring (considering the three moored instruments used in Figure 2 and Table 1) and glider RU06 are 0.05 and 0.11 °C for the gliders sampling the 500 m and 1 km boxes, respectively. Mean differences by height and glider deployment range from -0.04 to 0.083 °C and 0.87 to 0.15 °C for gliders sampling the 500 m and 1 km boxes, respectively (Table 1). The warm bias in moored T(z) observations has a clear height dependency, with the largest mean differences occurring at mid-height (11.6 m HAB). This is the case with T(z) comparisons for gliders sampling both the 500 m and 1km boxes, and in both 2012 and 2013 (Table 1). Reasons for the fairly consistent warm bias in the moored instruments are unknown but are possibly due to calibration differences between platforms and errors in diver estimates of instrument HAB. Temperature variance (σ^2) and its distribution was similar among the three T(z) measurement platforms. Values of σ^2 are 0.24, 0.26, and 0.27 °C for T(z) data from the glider sampling the 1 km box, the gliders sampling

the 500 m box, and the moored observations (considering the sampling heights in Table 1 and Figure 2).

Mean differences in T(z) measured with the glider and moored instruments show a clear dependence on glider box size (i.e. Table 1), as do the RMS difference and coefficient of determination (r^2). RMS differences in T(z) between the moored observations and those from the glider sampling a 1 km box pattern range from 0.21 to 0.30 °C, depending on HAB (Table 1). r^2 values considering the 1 km box pattern range from 0.34 to 0.46. By comparison, RMS differences and r^2 values considering the 500 m box glider tracks range from 0.08 to 0.29 °C and 0.26 to 0.69, respectively (Table 1). RMS differences are consistently larger, and r^2 values smaller for glider vs. mooring T(z) comparisons considering the 1 km box pattern. This is an expected result considering the increased distance between observations during the larger (1 km) box.

Comparisons between T(z) measured on counter-rotating gliders gives results similar to comparisons with the moored observations. RMS differences range from 0.07 to 0.20 °C and 0.14 to 0.35 °C in 2012 and 2013, respectively, for the discrete heights above bottom listed in Table 1. The largest RMS differences are observed near the surface, where T(z) range is greatest. RMS temperature differences between gliders are within 20% of those from the glider and mooring comparisons. Values of r^2 at the aforementioned discrete heights range from 0.45 to 0.71 in 2012 and 0.41 to 0.60 in 2013, consistent with the glider vs. mooring temperature comparisons. RMS differences and r^2 values over the entire water column are printed in Figure 3. Results ultimately indicate T(z) variations of O(0.1 C) exist on spatial scales of O(100 m) in the coastal ocean and the spatial differences exhibit statistically significant correlations in time. When configured as a mooring, glider T(z) data

deviates by O(0.1 C) from true mooring observations due to small differences in sampling characteristics that primarily include frequency and location.

Temperature results presented above and shown in Table 1 are computed using the "search" method (described in Section 2.4.1). Similar results were obtained using the "interpolation" method. T(z) values derived from both methods were linearly regressed and produced an r^2 value of 0.98.

3.2) Velocity

3.2.1) Velocity Sampling Intervals

The time over which glider velocity profiles are averaged is equivalent to the time from the beginning of a glider "dive" to the subsequent glider surfacing. This is a function of glider travel time between predefined surfacing locations or time since the previous surfacing (when a glider doesn't make it to the next surfacing location within some time predetermined time limit). For the 1 km box pattern, the mean time the glider spends underwater between surfacings is 42.4 minutes (σ = 20 minutes). For the 500 m box (averaged over all deployments) the mean time underwater between surfacings is 33.9 minutes (σ = 15.47 minutes).

The time between glider velocity profiles is also variable and depends on both the velocity averaging time and the time a glider spends at the surface transferring data. Mean times between average velocity measurements are 55 minutes (σ = 21.5 minutes) and 42 minutes (σ = 10.47 minutes) for the gliders sampling the 1 km and 500 m boxes (all deployments), respectively. As previously mentioned (section 2.4.1), all glider velocity profiles are defined to be at the midpoint in time between surfacings. Unlike temperature,

the time between velocity samples does not change with z because each velocity bin has the same timestamp for a given profile.

3.2.2) Vertically-averaged velocity results

Time series of $\mathbf{U}(t)$ (Equation 2) calculated from $\mathbf{u}_{G,DR,glider}$ (hereafter $\mathbf{U}(t)_{glider}$ as dead reckoned position is computed using the "glider" method) with $\alpha = 0°$ (the internal algorithm of the glider uses $\alpha = 0°$ as the default value when dead-reckoning position) shows pronounced oscillation in both the eastward and northward velocity components (Figure 4a). These oscillations are caused by an overestimate of $\mathbf{X}_{DR,glider}$ in the direction of glider motion. Thus, when the glider travels north/south $X_{DR,glider}$ is north/south of X_{GPS} and the poleward component of U(t) is overestimated/underestimated. Oscillations arise similarly for the eastward direction (Figure 4a) in a similar fashion. The oscillations ultimately arise because $\mathbf{u}_{G,DR,glider}$ with $\alpha = 0°$ does not accurately account for the glider drag caused by the externally mounted ADCP.

To account for the drag of the ADCP, a more accurate value of α is determined using velocity measured with the moored ADCP and a least squares approach. $\mathbf{U}(t)_{glider}$ is linearly regressed against $\mathbf{U}(t)$ from the mooring ADCP (Figure 5) to produce values of r^2 as a function of α. The "best" value of α (α_{best}) for each deployment is that which maximizes r^2 between the glider- and mooring-based components of $\mathbf{U}(t)$. Single α_{best} values are determined by averaging values computed separately for each velocity component (red and blue, in Figure 5). For both gliders in 2013 and RU06 in 2012, $\alpha_{best} = 3.7°$. For RU05 in 2012 $\alpha_{best} = 3.2°$.

Calculation of $\mathbf{U}(t)_{glider}$ using α_{best} instead of the default $\alpha = 0$ results in elimination of the velocity oscillations indicated above (Figure 4a vs. 4b; Figure 4b shows the effect of

including the calculated "best" value of α in calculations of $\mathbf{U}(t)_{glider}$ The bias in **U**(t) from using α = 0° occurs in both 2012 deployments and RU07 in 2013; time series of **U**(t) from these deployments are not shown but have similar patterns and values to those in Figure 4. The effect of using α_{best} is illustrated by calculating standard error ($\sigma * (\sqrt{N})^{-1}$ where N is the number of samples) and range of **U**(t) in Figure 4a and 4b. When applying α_{best} instead of α = 0, standard error in the u direction decreased to 0.0013 m s^{-1} (51% change) and 0.0043 m s^{-1} (21% change) in the v direction. For reference, standard error calculated from the moored ADCP was 0.0012 m s^{-1} and 0.0039 m s^{-1} in the u and v directions, respectively. Range calculated using α_{best} was 0.091 m s^{-1} (43% change from α = 0) and 0.2899 m s^{-1} (21% change) in the u and v directions, respectively. These values of dynamic range from $\mathbf{U}(t)_{glider}$ are both within 10% of the ranges reported from the mooring. While the statistics of $\mathbf{U}(t)_{glider}$ listed above are all from RU06, very similar results are obtained for the other gliders used in this study. The large errors associated with using α = 0 and the "eye-test" of Figure 4 underscore the importance of properly estimating angle of attack in calculations of current velocity.

Vertically averaged velocity calculated by using the $\mathbf{u}_{G,DR,beam}(t)$ and $\mathbf{u}_{G,DR,ENU}(t)$ are not as sensitive to angle of attack as $\mathbf{u}_{G,DR,glider}(t)$. For example, Δr^2 of U(t), V(t) for α = 0° to α = 3.7° for the "ENU" method is 0.003, 0.021 beam for V(t), U(t) respectively. Similarly for the "beam" method Δr^2 = 0.022, 0.015 for V(t), U(t), respectively. The "glider" method has Δr^2 of 0.14, and 0.35 for V(t), U(t), respectively. The order of magnitude difference in agreement between glider-derived and mooring-derived velocities with the assumption α = 0° indicates that $\mathbf{u}_{G,DR,glider}$ provides poorer measurements of **U**(t) if angle of attack is unknown. However, if angle of attack can be estimated, the "glider" method of dead-

reckoning glider position yields results of **U**(t) that correlate best with those from the mooring.

An additional bias in **U**(t) was also observed after the angle of attack correction, most notably in the time series of **U**(t) found by using $\mathbf{u}_{G,DR,beam}(t)$ and $\mathbf{u}_{G,DR,ENU}(t)$ (see figure 4c,d). A slight "dip" occurs every 4^{th} point around 9 August, 2012 in V(t) of figure 4c and 4d when the glider was traveling on a north-south transect of the box, the same direction as the prevailing currents. The bias in measurements of currents in the same direction as the motion of a glider (or AUV) is a well known phenomenon (see Fong and Monismith, 2004) and the "dips" of equartorward flow observed in this study are O5 cm s^{-1} consistent with Fong and Monismith (2006). We experimented with different ADCP bins (see Jaramillo and Pawlak, 2010 for more information) as well as averaging multiple ADCP bins together in our calculations of $\mathbf{u}_{G,DR,beam}(t)$ and $\mathbf{u}_{G,DR,ENU}(t)$. Altering the bins used did not increase r^2 or reduce the dips in figure 4d, so the two bins nearest the glider ADCP are used throughout this analysis.

3.2.2) Vertically-resolved velocity results

The **u**'(z,t) term from the glider's ADCP in equation 4 compared with the **u'**(z,t) from the moored ADCP data showed greater agreement during the sampling of the 500 m box compared to the 1 km box. For RU06, u'(z,t) and v'(z,t) r^2 decreased from 0.745 and 0.774 respectively for the 500 m box to 0.520 and 0.570 in the 1 km box when examining the whole water column. For all 500 m boxes, the mean value of r^2 is 0.771 ± 0.051. The **u**'(z,t) of the glider and mooring generally are in good agreement during the time interval between surfacings (figure 6a and 6b). Velocities near the surface (>21 m) and near the bottom (<3 m) have been removed due to side-lobe effects and limited data availability,

respectively. Figure 6c and 6d show a linear regression of u'(z,t) and v'(z,t) from the glider-ADCP velocities and those from the mooring ADCPs (see figure 7 for regression plots, RMS differences, and mean values from all deployments). It is notable that while r^2 varies with HAB, RMS differences do not and are < 5 cm s^{-1} which shows consistency between platforms.

We hypothesize the lower correlation coefficients in the 1 km box are due to spatial variability of the current field and the longer averaging time of the 1 km box. Mean and RMS differences are of O2 cm s^{-1} for all box sizes and do not have a height above bottom dependency. These results confirm the effectiveness of the methods of Todd et al (2011) and indicate the importance of virtually mooring gliders in a smaller geographic area to best reproduce the results of a moored ADCP. Given the lower r^2 and similar RMS for the 1 km box, experimental design may dictate that a 1 km box is sufficient.

3.3.3) Absolute, height-resolved velocity results

Calculations of the absolute, height-resolved velocity, **u**(z,t) (equation 4) have similar trends in correlation and variance to **u'**(z,t) and **U**(t) discussed above. All results of **u**(z,t) presented in this section are calculated using $\mathbf{U}(t)_{glider}$. Measurements of v(z,t) from the glider-ADCP better correlate with the mooring velocities than u(z,t) due to an increased variance in along-shore velocities. RMS differences in u(z,t) and (z,t) are O3 cm s^{-1} for the 1km and 500 m box and do not have an HAB dependency. The small differences in velocity measured by the glider-mounted ADCP and bottom-mounted ADCP imply that gliders used as virtual moorings in both 500 m and 1 km box closely reproduce currents measured by a traditional moored ADCP.

Contours (figure 8-10) and time series (figure 11, 12) of velocity data illustrate the similarity of glider-derived velocity profiles compared with those from the moored ADCP. The contours of velocity show similar flow regimes between glider and mooring; both observe a burst of poleward flow throughout the water column on day three in figure 8c, d. Some finer features which appear in mooring data are not resolved in the glider due to a sparseness of measurements (see figure 11). In figure 11, 12, the 3 HAB are chosen to be consistent with the heights of the moored instruments analyzed in section 3.1. Similar patterns are observed by the glider and mooring (figure 11a, b, c) in the 500 m and 1 km box which shows the agreement in currents measured by the glider ADCPs and moored ADCP. This further indicates that virtually mooring gliders in a 500 m box pattern provides accurate measurements of velocity, and that small scale variations on the order of 1 km (Ohlmann et al, 2012) lower agreement between gliders shown in figure 13. Side-lobe effects near the surface cause the lower agreement from about 21 m HAB and up.

To assess the consistency of current measurements from the glider ADCPs, linear regressions of glider versus glider were also computed for the two day period when the gliders were collocated in 2012. Comparisons are made using the "search method" with windows of ± 0.5 m and ± 20 minutes. The longer time window (compared to temperature) is used due to the longer averaging times of velocity and the fact that the gliders are not sampling the vertical synchronously. Values of r^2 of $\mathbf{u}(z,t)$ measured by the gliders were 0.758 for the along-shore component and 0.623 in the cross-shore direction over the entire water column and RMS differences in u(z,t) and (z,t) are similar to comparisons with the mooring, O(3 cm s^{-1}). While correlation is affected by box size, RMS differences are not. In

all deployments, correlation is significant and RMS differences are low which we take to mean that we can successfully use gliders as virtual moorings to measure currents.

4) Discussion

4.1 Glider position underwater

The verity of current observations from a glider mounted ADCP largely depends on computation of a glider's dead-reckoned position ($\mathbf{X}_{DR}(t)$; Equation 2). Determining the optimum manner for calculating $\mathbf{X}_{DR}(t)$ requires "ground truth" of a glider's velocity relative to the Earth ($\mathbf{u_G}(t)$). This ground truth has typically come from either "bottom tracking" the glider, or from observations after reversing the glider direction (hereafter "turnaround") so the net effect of ocean currents on integrated glider motion is zero. Here we suggest comparison with moored ADCP observations to find the optimal glider angle of attack as a third method for improving a gliders dead reckoned position. This method avoids the need for a downward looking glider ADCP and/or the possibly erroneous assumption of flow stationarity. It does however require that a glider be flown in the vicinity of a moored ADCP.

Bottom tracking involves measuring the "motion" of the seafloor relative to the moving glider (essentially the glider motion relative to the stationary bottom). This requires a downward looking ADCP with beams that reach the ocean bottom. While bottom tracking can help reduce errors in current observations from a horizontally moving ADCP, it does not provide constant and exact horizontal platform motion (e.g. Visbeck 2002). Further, as pointed out by Pettigrew et al. (2014), there is often a tradeoff between bottom tracking and upper ocean observations (depending on ADCP frequency and water depth). Glider ADCPs in this study are upward looking to maximize data quantity near the surface.

Bottom tracking has been shown to reduce glider position (and thus glider ADCP current observation) errors, but not eliminate them (Fong and Jones 2006, Jaramillo and Pawlak 2010, Ordonez 2012, Ordonez et al 2012). Root mean squared differences between currents from glider and moored ADCPs decreased from ~6 to ~4 cm/s when bottom tracking is considered (Ordonez 2012). This result is from the comparison of roughly 2.5 hours of glider ADCP data from a single glider dive roughly 3 km from the moored ADCP off the Oregon coast. The comparison is for depth-average currents with velocities near 10 cm/s (or less). By comparison, RMS differences in our study range from 4.26 to 5.07 cm/s (considering the different glider deployments) when glider ADCP velocities are computed with $\alpha = 0°$. Using $\alpha = 3.7°$ (the angle of attack that maximizes the correlation between velocities from glider and moored ADCPs; 3.2° for RU05 in 2012) reduces RMS velocity differences to between 2.13 and 2.69 cm/s. Dead reckoning with an ideal angle of attack gives RMS glider-mooring velocity differences that are nearly 50% smaller than those presented by Ordonez (2012) using bottom tracking.

The "turnaround" method (Pollard and Reed 1989, Todd et al. 2011) is based on a correction factor to $\mathbf{u}_g$ (the glider's velocity through the water) that forces $\mathbf{U}(t)$ (the vertically averaged velocity of the water) to be constant between observations from reversing glider transects. The method assumes ocean currents are homogeneous and stationary within the location and time of the glider reversal. An uncertainty in $\mathbf{u}_g$ of only $O(1\ cm\ s^{-1})$ is reported by Todd et al (2011) using this method. However, the small correction factors reported by Todd et al (2011) are not relevant to coastal observations such as those presented here. Todd et al (2011) use data well offshore where the glider dives to 500m and currents are expected to be largely geostrophic. Further, averages are over 1 day

so that tidal and inertial signals are eliminated. Submesoscale processes that can dominate in the coastal ocean are inconsistent with the assumption of a constant flow field making the turnaround method undesirable for coastal ocean studies in relatively shallow water.

4.2 Glider angle of attack

Dead-reckoned glider position is typically computed by internal glider algorithms with $\alpha = 0°$ (REFERENCE TWR operations manual). This ultimately results in an overestimate of glider speed through the water, compared with $\alpha > 0°$ (Equation 5). Considering average dp/dz and θ values of 14 cm/s and 23.5 deg respectively, increasing α from 0 to 3.7° results in a decrease in $\mathbf{U}_g$ by nearly 5 cm/s. A similar calculation by Merckelbach et al. (2001) indicates an overestimate of $\mathbf{U}_g$ by ~3cm/s if $\alpha = 1.6°$ is ignored. Previous estimates of α range from 2 to 3° (Sherman et al 2001, Cooney 2011). These values consider a glider with internally mounted ADCP, presumably giving less drag (and thus a smaller α) than with an externally mounted instrument. The α values computed in our experiments are slightly larger than previously reported, consistent with increased drag associated with an externally mounted ADCP.

Accurate determination of α in this study depends on some reference ocean current measurement; in this case a moored ADCP. Ideally, future glider missions that make ADCP measurements would spend some time flying nearby moored current measurements so that α could be accurately determined for the given glider configuration and environmental conditions following the least-squares method presented here. In the absence of reference currents, the previously established α for a glider configuration could be used. Results of this study indicate that if α for a particular glider configuration is not known, $\mathbf{U}_{G,DR}$ is best

determined from the ADCP data themselves using the "beam" or "enu" methods for computing $\mathbf{U}_{G,DR}$ as these methods are much less sensitive to an erroneous α compared with the "glider" method. Increasing α from 0 to 3.7° results in $\mathbf{U}_{G,DR,beam}$ and $\mathbf{U}_{G,DR,enu}$ decreases of only 0.72 and 0.5 cm/s, respectively (compared with 4.2 cm/s for the glider method).

4.3 **Glider direction relative to the ocean currents**

The dependence of ADCP ocean water velocity measurements on the direction of instrument motion has been previously observed by Fong and Monismith (2004) from coastal ocean data collected off the California coast. In that study, the ADCP was mounted on a ship, not a glider, and bottom-tracking was utilized. When the ship moved in the down-current direction the ADCP velocity observations overestimated the water, and visa-versa. The net bias reported by Fong and Monismith (2004) at times exceeds 10 cm/s in a water column moving at a similar velocity. This can ultimately result in the moving ADCP getting the current direction incorrect. Despite a very accurate bottom-tracking system, the ADCP observations still showed a significant bias (overestimate) in water velocity that is in the direction of ADCP motion. The Fong and Monismith (2004) study thoroughly quantifies the bias and suggests overcoming it by steaming in a direction orthogonal to the current direction. No explanation for the bias is provided by Fong and Monismith (2004), although avenues for further investigation are suggested.

Incorporating the optimal for angle of attack in calculations of vertically averaged velocity reduces the bias in the direction of the glider's motion, but does not completely eliminate it (Figure 4a, 4b; section 3.2.2). To examine the directional bias, we analyzed changes in RMS velocity differences as a function of the direction the glider was traveling.

With $\alpha = 0°$, RMS velocity differences in the U direction calculated from $\mathbf{U_{G,DR,Glider}}$ are 1.54, 3.98, 2.3 and 4.3 cm s^{-1} when the glider travels north, east, south, west, respectively. Note the higher RMS differences in the U direction when the glider is going east and west. Similarly, with $\alpha = 0°$, RMS velocity differences in the V direction are 4.7, 3.6, 4.46, 2.69 cm s^{-1} when the glider travels north, east, south, west, respectively. Here, higher RMS velocity differences in the V direction are found when the glider is traveling north and south (the direction parallel to the V direction).

As discussed previously (section 3.2.2), using $\alpha = 3.7°$ (or α best) has a greater effect on velocities calculated using $\mathbf{U_{G,DR,Glider}}$ than the two other methods. The ΔRMS in the U direction between velocities that use α best and $\alpha = 0°$ are 0.11, 2.98, 0.0085, 2.9 cm s^{-1} when the glider travels north, east, south, west, respectively. Similarly, in the V direction ΔRMS are 3.23, 1.49, 1.29, 0.85 cm s^{-1} when the glider travels north, east, south, west, respectively. When using $\mathbf{U_{G,DR,beam}}$, RMS velocity differences in the U and V direction are all < 2.57 cm s^{-1} and ΔRMS are all < .25 cm s^{-1}. Figure 14 shows the effect of using α best and $\alpha = 0°$ on RMS velocity differences for different directions. Similar to Fong and Monismith (2004) we cannot explicitly correct for the bias of current estimates in the direction of motion. However, by using the optimal angle of attack, RMS velocity differences are <2 cm s^{-1}, in the direction perpendicular to the dominate flow and are not directionally biased. Currents measured parallel to the dominate flow direction (southward in this study) do show a bias and have RMS velocity differences of < 4 cm s^{-1}. The large drop in RMS velocity difference in the V direction when the glider is going north (blue bars figure 14b, d) is notable and is caused by the improved accuracy of dead-reckoned position

by using α best. The effect is less noticeable when the glider travels south (green bars in figure 14b, d) due to the prevailing currents making dead-reckoned estimates less accurate.

After removing velocities near the surface and bottom (section 3.2.2), RMS differences are O(3 cm s^{-1}) which is the same magnitude as Todd et al (2011). Todd et al (2009) calculate vertically averaged currents from spray gliders to be 5.4 % larger and 0.8° different from a nearby mooring in 57 m water. Using equation C1 from Todd et al (2009), we calculate glider-ADCP estimates of **U**(t) to be an average of 5.5 % greater than moored-ADCP estimates, and a mean difference in direction of 1.02°.

5) Conclusions

The use of gliders as virtual moorings in box patterns instead of the more conventional single-station approach appears to offer advantages for ocean observing. Using a box pattern 500 m to a side allows for spatial sampling of 0.25 km^2 instead of the much smaller area associated with repeated sampling of a single location. The 500 m box also appears to be optimal for monitoring small-scale variability. As shown, expanding the box to 1 km a side increases the sample area by a factor of 4 but decreases the correlation between glider and mooring measurements, particularly with respect to temperature.

We have shown in this study the necessity of estimating angle of attack for each deployment of a glider by comparison with independent measurements of velocity. Additionally, if no estimate of angle of attack can be made, we recommend a value of angle of attack and two alternate methods of dead-reckoning the glider's velocity that are not as sensitive to changes in angle of attack. Our results improve upon existing methods and provide new techniques for processing glider-as-mooring data sets. Furthermore, we have

demonstrated that correlations of our results with a bottom-mounted ADCP are statistically significant.

References

Brumley, B. H., Cabrera, R. G., Deines, K. L., & Terray, E. A. (1991). Performance of a broad-band acoustic Doppler current profiler. *Oceanic Engineering, IEEE Journal of, 16*(4), 402-407.

Castelao, R., Schofield, O., Glenn, S., Chant, R., & Kohut, J. (2008). Cross-shelf transport of freshwater on the New Jersey shelf. *Journal of Geophysical Research, 113*(C7), C07017

Chelton, D. B. (1983). Effects of sampling errors in statistical estimation. *Deep Sea Research Part A. Oceanographic Research Papers*, *30*(10), 1083-1103.

Chiodi, A. M., & Eriksen, C. C. (2002). Geostrophic fjord exchange flow observed with seaglider autonomous vehicles. *Journal of Physical Oceanography*.

Davis, R. E., Eriksen, C. C., & Jones, C. P. (2003). Autonomous buoyancy-driven underwater gliders. *The technology and applications of autonomous underwater vehicles*, 37-58.

Davis, R. E., Ohman, M. D., Rudnick, D. L., Sherman, J. T., & Hodges, B. (2008). Glider surveillance of physics and biology in the southern California Current System. *Limnology and Oceanography*, *53*(5), 2151-2168.

Dickey, T. D., Itsweire, E. C., Moline, M. A., & Perry, M. J. (2008). Introduction to the Limnology and Oceanography Special Issue on Autonomous and Lagrangian Platforms and Sensors (ALPS). *Limnol. Oceanogr*, *53*(5 part 2), 2057-2061.

Dickey, T. (2009). Progress in multidisciplinary sensing of the 4-dimensional ocean. In *SPIE Defense, Security, and Sensing* (pp. 731702-731702). International Society for Optics and Photonics.

Dickey, T. D., E. C. Itsweire, M. A. Moline, and M. J. Perry (2008), Introduction to the Limnology and Oceanography Special Issue on Autonomous and Lagrangian Platforms and Sesnors (ALPS), Limnol. Oceanogr., 53(2), Part 2, 2057 – 2061.

Eriksen, C. C., Osse, T. J., Light, R. D., Wen, T., Lehman, T. W., Sabin, P. L., and Chiodi, A. M. (2001). Seaglider: A long-range autonomous underwater vehicle for oceanographic research. *Oceanic Engineering, IEEE Journal of*,*26*(4), 424-436.

Eriksen, C. C., & Perry, M. J. (2009). The nurturing of seagliders by the National Oceanographic Partnership Program. *Oceanography*, *22*(2), 146.

Fratantoni, D. M., & Lund, J. M. (2006). Glider operations in Buzzard's Bay, MA. *Woods Hole Ocean. Inst., Tech. Rep. BUZZ0306*.

Graver, J. G., Bachmayer, R., Leonard, N. E., & Fratantoni, D. M. (2003, August). Underwater glider model parameter identification. In *Proceedings of the 13th International Symposium on Unmanned Untethered Submersible Technology*.

Griffiths, G., Davis, R., Eriksen, C., Frye, D., Marchand, P., & Dickey, T. (2001). Towards new platform technology for sustained observations. *Observing the ocean for climate in the 21st century. GODAE, Bureau of Meteorology*, 324-338.

Hickey, B. M.. The California Current system-hypotheses and facts, Prog. Oceanogr.. 8. 191-279, 1979.

Hodges, B. A., & Fratantoni, D. M. (2009). A thin layer of phytoplankton observed in the Philippine Sea with a synthetic moored array of autonomous gliders. *Journal of Geophysical Research*, *114*(C10), C10020.

Horne, E. P. and J. M. Toole (1980), Sensor Response Mismatches and Lag Correction Techniques for Temperature-Salinity Profilers, J. Phys. Oceanogr., 10(7), 1122 – 1130.

Isaaks, E. H, and R. M. Srivastava (1989), An Introduction to Applied Geostatistics, pp. 278 – 322, Oxford University Press, Inc., New York.

Jaramillo, S., & Pawlak, G. (2010, September). AUV-based observations of rough bed hydrodynamics. In *Autonomous Underwater Vehicles (AUV), 2010 IEEE/OES* (pp. 1-9). IEEE.

Lynn, R. J., & Simpson, J. J. (1987). The California Current System: The seasonal variability of its physical characteristics. *Journal of Geophysical Research*, *92*(C12), 12947-12.

Mensah, V., M. Le Menn, and Y. Morel (2009), Thermal Mass Correction for the Evaluation of Salinity, J. Atm. and Ocean. Tech., 26, 665 – 672.

Mahoney, K. L., Grembowicz, K., Bricker, B., Crossland, S., Bryant, D., Torres, M., & Giddings, T. (2009). RIMPAC 08: Naval Oceanographic Office Glider Operations. In *SPIE Defense, Security, and Sensing* (pp. 731706-731706). International Society for Optics and Photonics.

Merckelbach, L. M., Briggs, R. D., Smeed, D. A., & Griffiths, G. (2008, March). Current measurements from autonomous underwater gliders. In *Current Measurement Technology, 2008. CMTC 2008. IEEE/OES 9th Working Conference on* (pp. 61-67). IEEE.

Ohlmann, J. C., LaCasce, J. H., Washburn, L., Mariano, A. J., & Emery, B. (2012). Relative dispersion observations and trajectory modeling in the Santa Barbara Channel. *Journal of Geophysical Research: Oceans (1978–2012)*,*117*(C5).

Pettigrew, N. R., Neary, M., Fleming, R., & Fikes, C. P. (2014). Evaluations of a 600 kHz RDI phased array system ADCP and a wave module operating on a G2 Slocum glider. In *Oceans-St. John's, 2014* (pp. 1-7). IEEE.

Robbins, I. C., G. J. Kirkpatrick, S. M. Blackwell, J. Hiller, C. A. Knight, and M. A. Moline (2006), Improved monitoring of HABs using autonomous underwater vehicles (AUV), Harmful Algae 5, 749 – 761.

Rudnick, D. L., and S. T. Cole (2011), On sampling the ocean using underwater gliders, J. Geophys. Res., 116, C08010, doi:10.1029/2010JC006849.

Rudnick, D. L., Davis, R. E., Eriksen, C. C., Fratantoni, D. M., & Perry, M. J. (2004). Underwater gliders for ocean research. *Marine Technology Society Journal*, *38*(2), 73-84.

Ryan, J. P., A. M. Fischer, R. M. Kudela, M. A. McManus, J. S. Myers, J. D. Paduan, C. M. Ruhsam, C. B. Woodson, and Y. Zhang (2010), Recurrent frontal slicks of a coastal ocean upwelling shadow, J. Geophys. Res., 115, C12070, doi:10.1029/2010JC006398.

Sherman, J., R. E. Davis, W. B. Owens, and J. Valdes, 2001: The autonomous underwater glider “Spray”. IEEE J Oceanic Eng. 26:437-446.

Terray, Eugene A., Blair H. Brumley, and Brandon Strong. "Measuring waves and currents with an upward-looking ADCP." *Current Measurement, 1999. Proceedings of the IEEE Sixth Working Conference on*. IEEE, 1999.

Todd, R. E., Rudnick, D. L., Mazloff, M. R., Davis, R. E., & Cornuelle, B. D. (2011). Poleward flows in the southern California Current System: Glider observations and numerical simulation. *Journal of Geophysical Research: Oceans (1978–2012)*, *116*(C2).

van Haren, H. (2001). Estimates of sea level, waves and winds from a bottom-mounted ADCP in a shelf sea. *Journal of Sea Research*, *45*(1), 1-14

Visbeck, M. (2002). Deep Velocity Profiling Using Lowered Acoustic Doppler Current Profilers: Bottom Track and Inverse Solutions*. *Journal of Atmospheric and Oceanic Technology*, *19*(5), 794-807.

Weller, R. A., D. L. Rudnick, N. J. Pennington, R. P. Trask and J. R. Valdes. 1990. Measuring upper ocean variability from an array of surface moorings in the subtropical convergence zone. J Atmos Oceanic Technol. 7:68-84.

Figure 1a

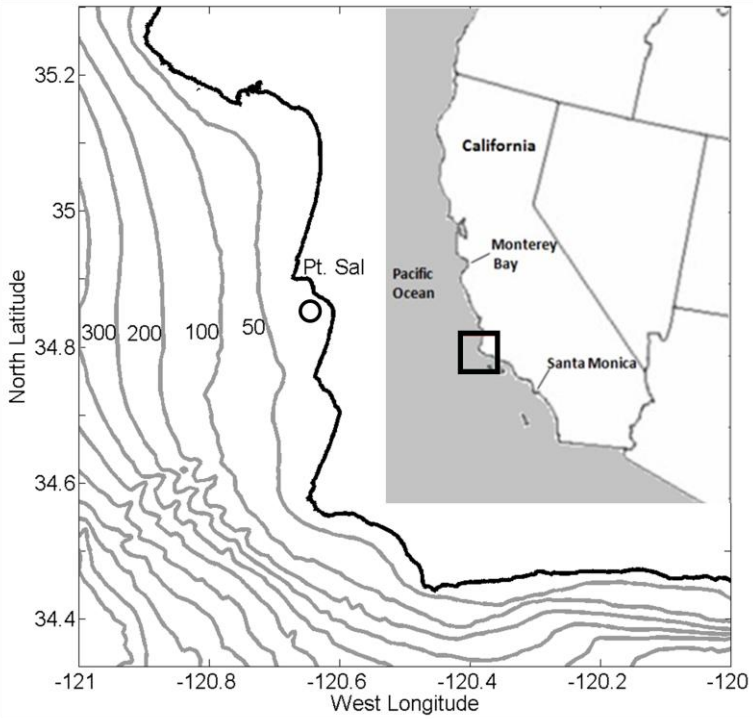

Figure 1a: Map of the study area in California, USA. The black box in the inset shows the approximate study region bounded by gray box. Gray lines indicate bathymetric contours at 50 m and then 100 m increments. The black circle indicates the location of the mooring and gliders.

Figure 1b

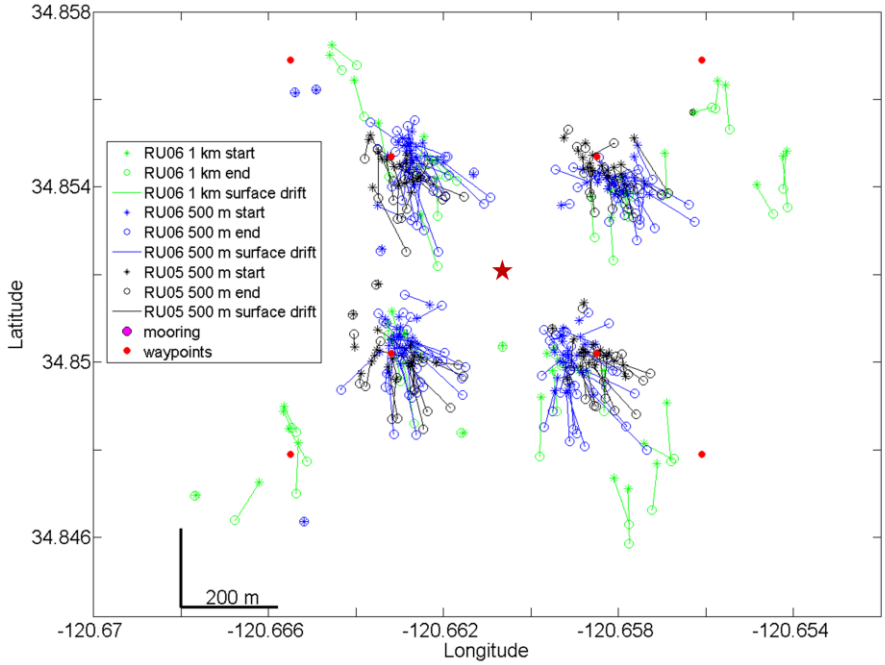

Figure 1b: Map of glider positions with waypoints (filled red circles) and the mooring (red star). The various flight paths are represented by different colors, where green represents the RU06 1km path, blue represents the RU06 500m path, and black represents the RU05 500m path. The lines represent the overall drift of the glider while on the surface and connect the initial GPS position (asterisk) with the final GPS position (open circle) before diving. These lines indicate the direction of surface drift, but do not imply linear drift.

Figure 2

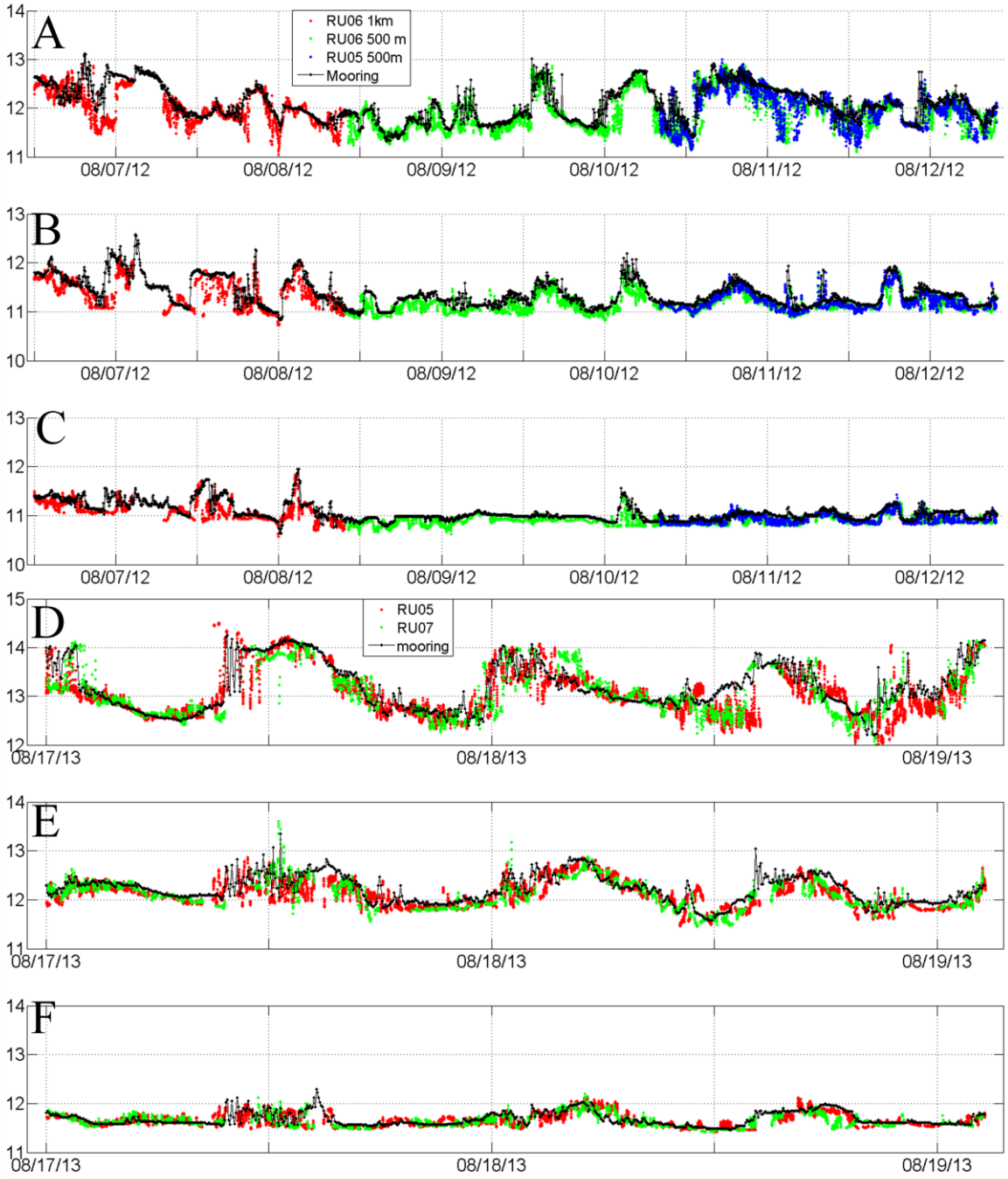

Figure 2: In 2012 (panels A-C), RU06 sampled a 1 km box (red), a 500 m box (green), and RU05 a 500 m box (blue). In 2013 (panels D-F) RU05 (red) and RU07 (green) each sampled a 500 m box. T(z) from moored thermistors are shown as a black curve in all panels. Data are shown at z = 20.4 m (A,D), z= 11.6 m (B, E), and z = 6.7 m (C, F).

Figure 3

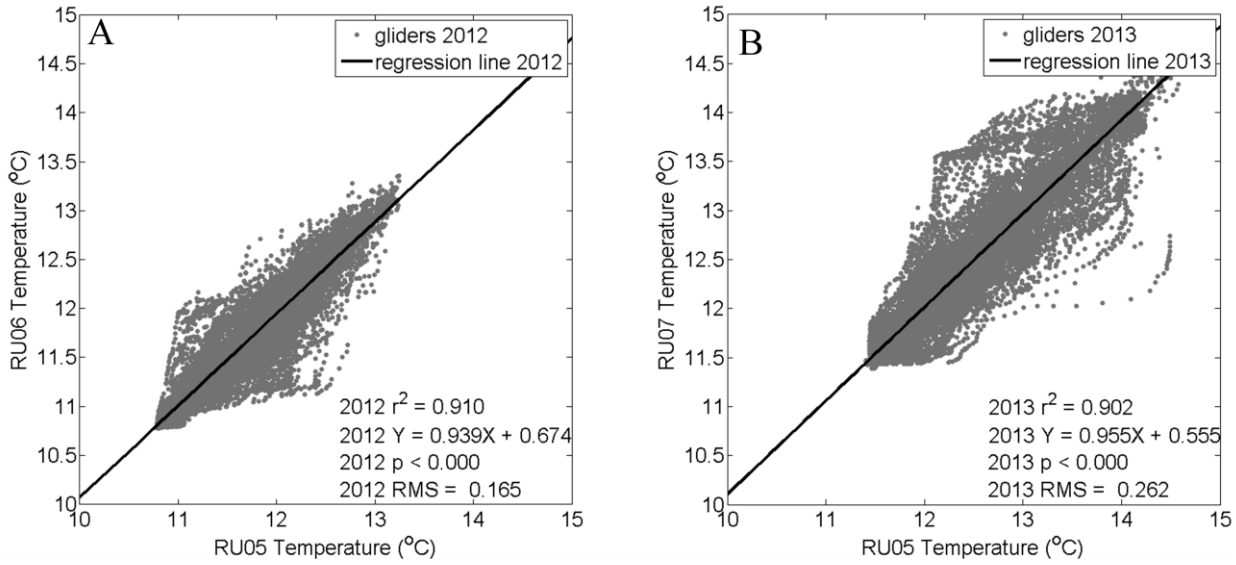

Figure 3: Linear regression of temperatures from gliders (see axis labels) for the period 08/10/12 to 08/12/12 (A) and 08/17/13 to 08/19/13 (B) when the gliders were collocated. Each glider point is found using a "search" window of .25 m and 1 minutes.

Figure 4

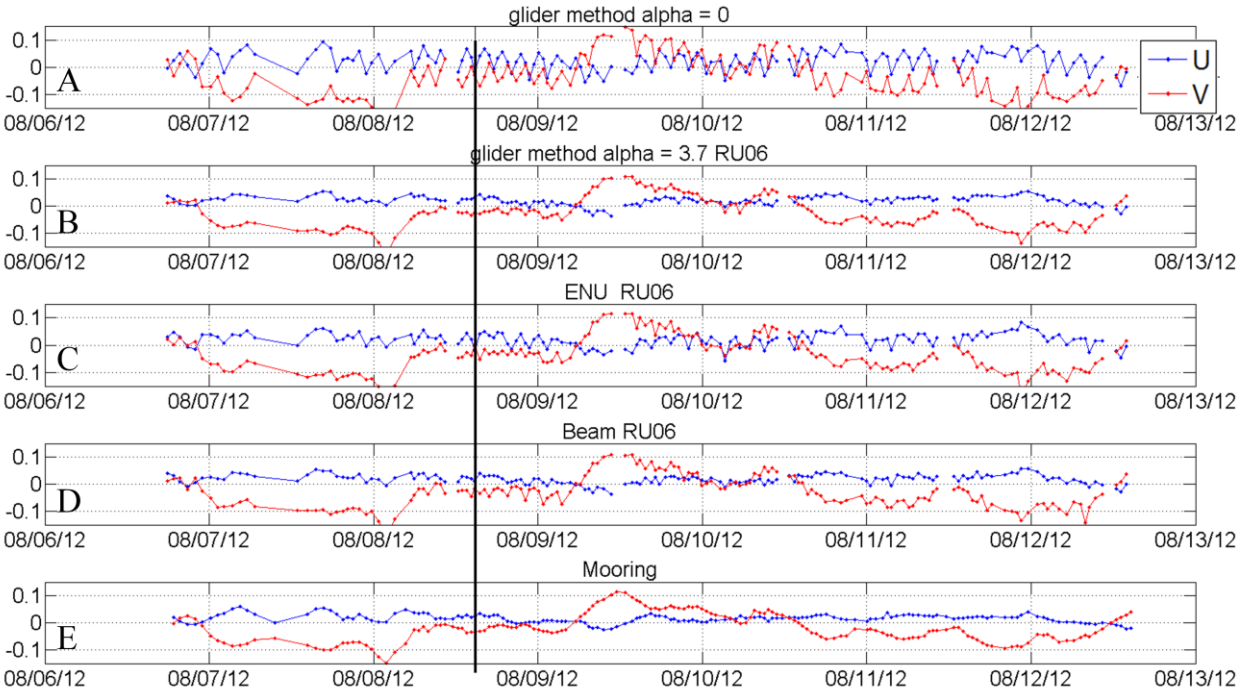

Figure 4: Time series of vertically-averaged velocity (U(t)) in the u (blue) and v (red) directions from the different methods of dead-reckoning position in section 2.4.3. A) "glider" method with α = 0. B) "glider" method with α = 3.7. C) The "ENU" method. D) The "beam" method. E) Currents from the bottom-mounted ADCP averaged over the same time interval as the glider data in panels A-D. The vertical black line indicates the switch from 1 km to 500 m box.

Figure 5

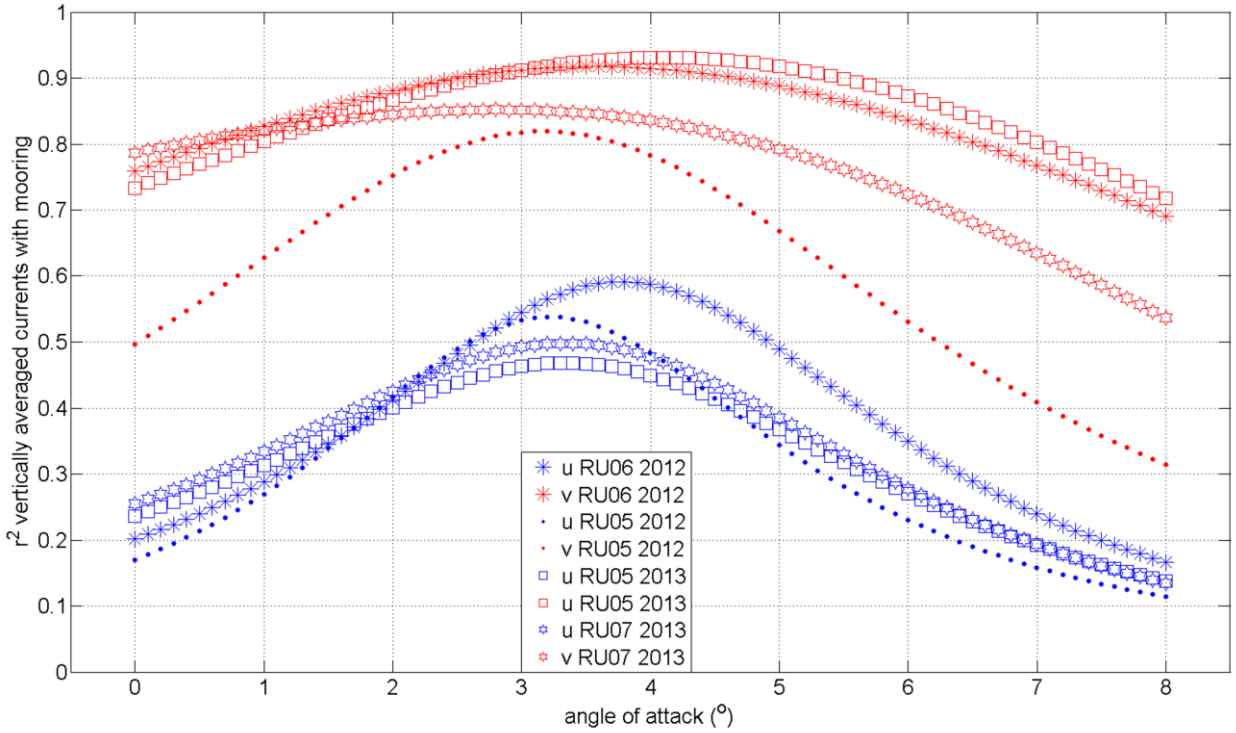

Figure 5: r^2 of vertically averaged velocity from the "glider" method versus vertically averaged velocity from the moor ADCP on the y-axis. Different values of α used in the "glider" method are on the x-axis. Blue shapes indicate r^2 in the U, onshore direction, and red indicate r^2 in the V, alongshore direction. Legend denotes individual deployments

Figure 6

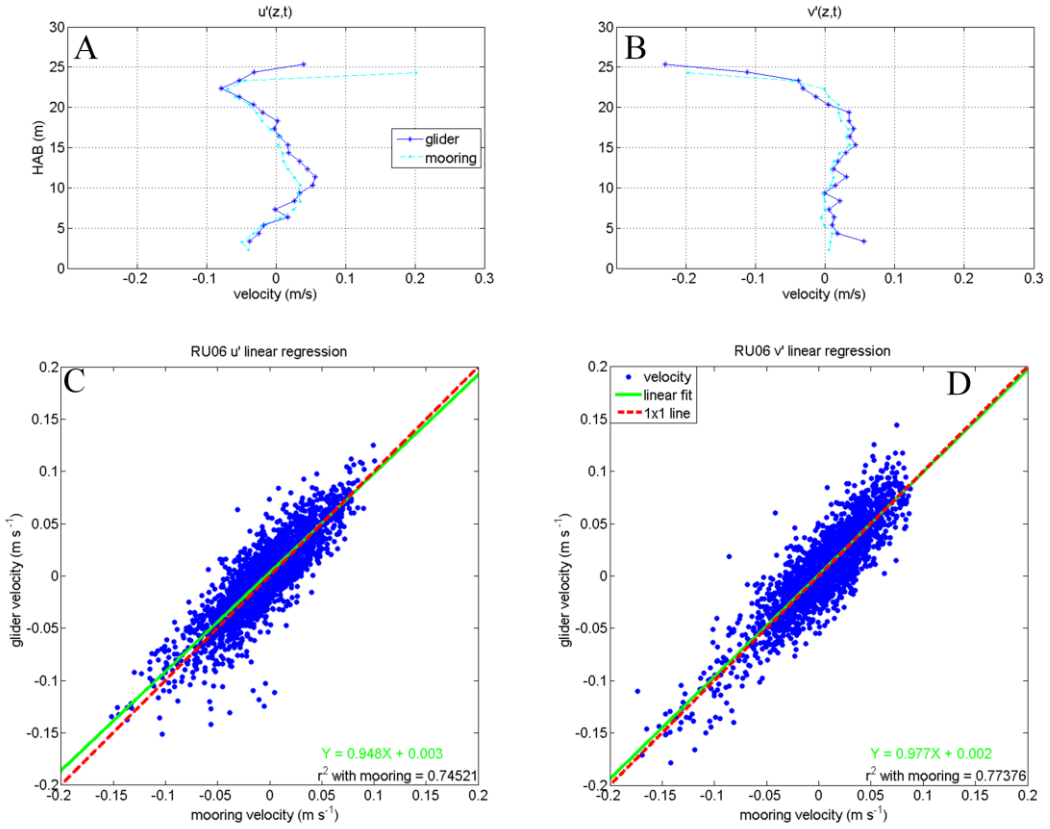

Figure 6: An example vertical profile of u' (A) and v' (B) from the glider ADCP (blue) and the moored ADCP (cyan). Linear regressions of u' (C) and v' (D) for the data during RU06's 500 m flight. Green line is a linear fit, and red line has a slope of 1 for comparison.

Figure 7

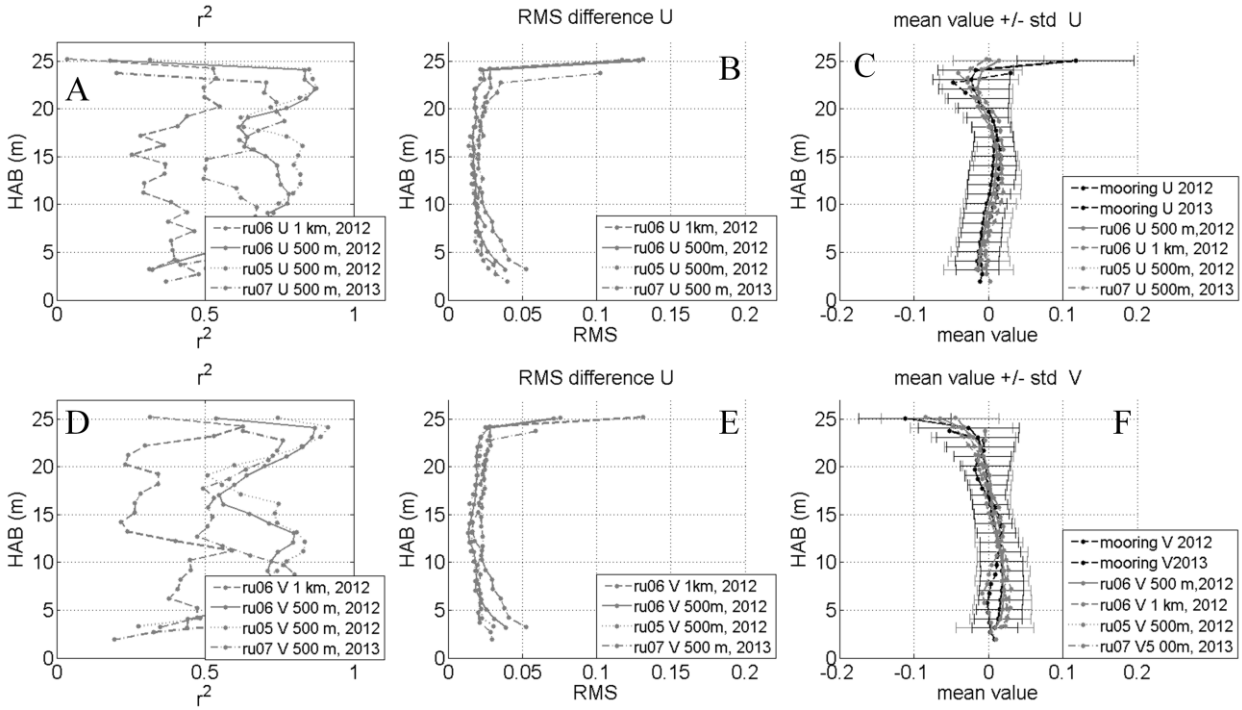

Figure 7: Vertical profiles of r^2 (A), RMS difference (B) and mean value +/- one standard deviation displayed as horizontal error bars (C) of u'(z,t). Vertical profiles of r^2 (D), RMS difference (E) and mean value (F) +/- one standard deviation of v'(z,t) are shown in the bottom row. Standard deviations are very similar between deployments so, for clarity, only one set of error bars for the glider and mooring are shown in C and F.

Figure 8

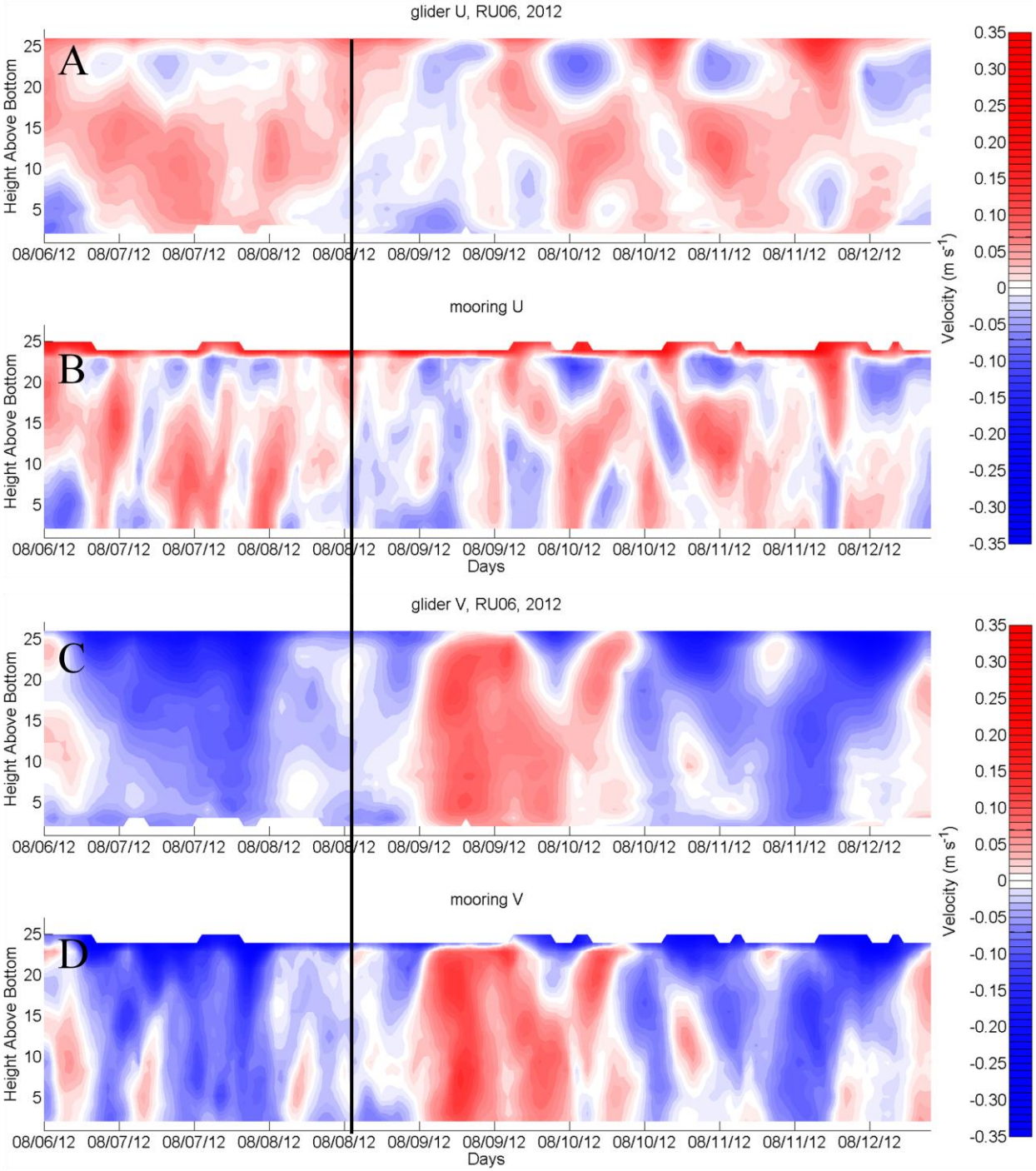

Figure 8: Contour of u(z,t) **from the glider RU06 (A) and mooring (B) and** v(z,t) **from the glider RU06 (C) and mooring (D). Vertical black line indicates shift from 1 km box to 500 m box of glider RU06 in 2012.** U **and** V **are positive (red) in the onshore and poleward directions, respectively.**

Figure 9

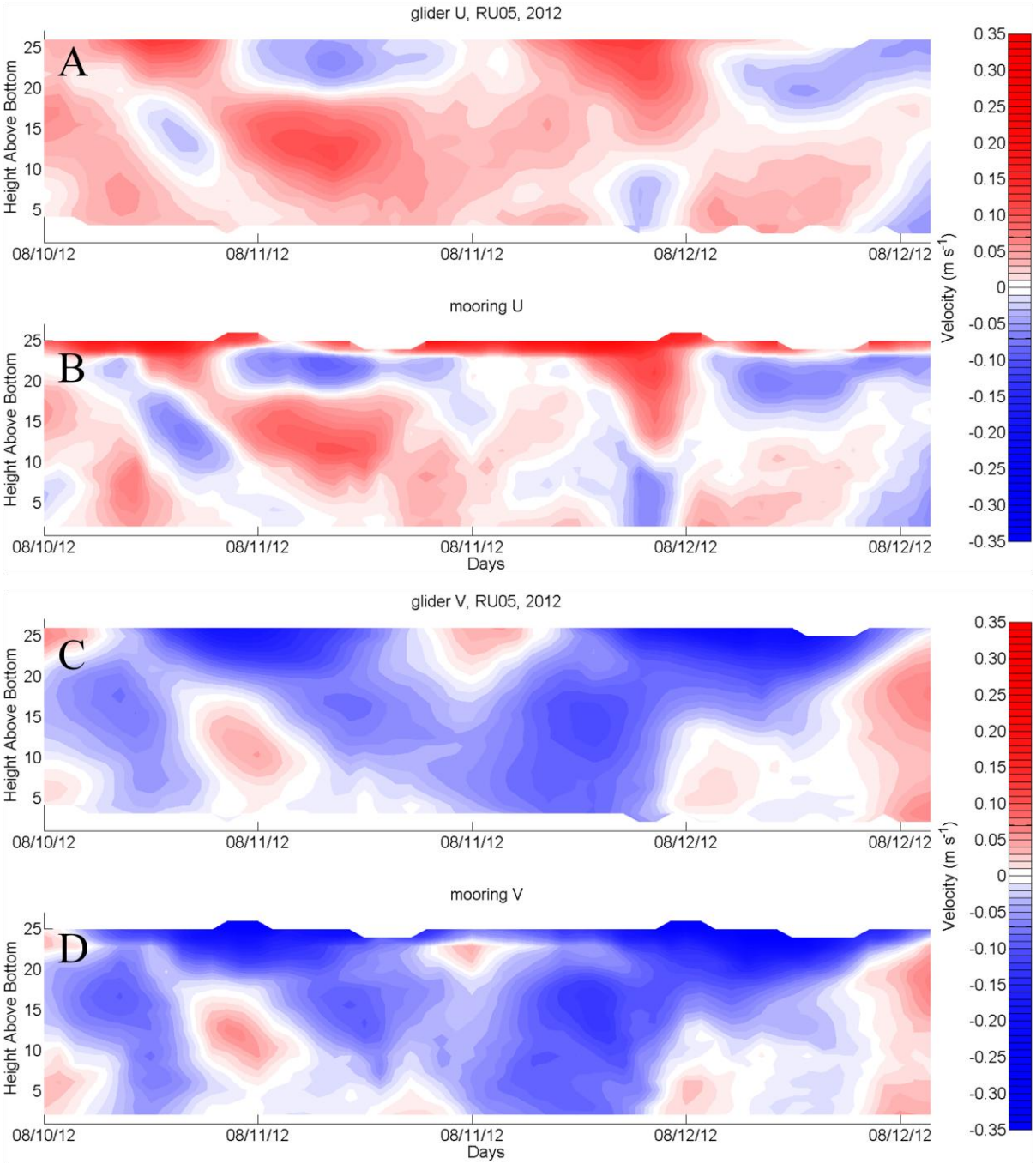

Figure 9: Contour of u(z,t) **from the glider RU05 (A) and mooring (B) and** v(z,t) **from the glider RU05 (C) and mooring (D) in 2012.** U **and** V **are positive (red) in the onshore and poleward directions, respectively.**

Figure 10

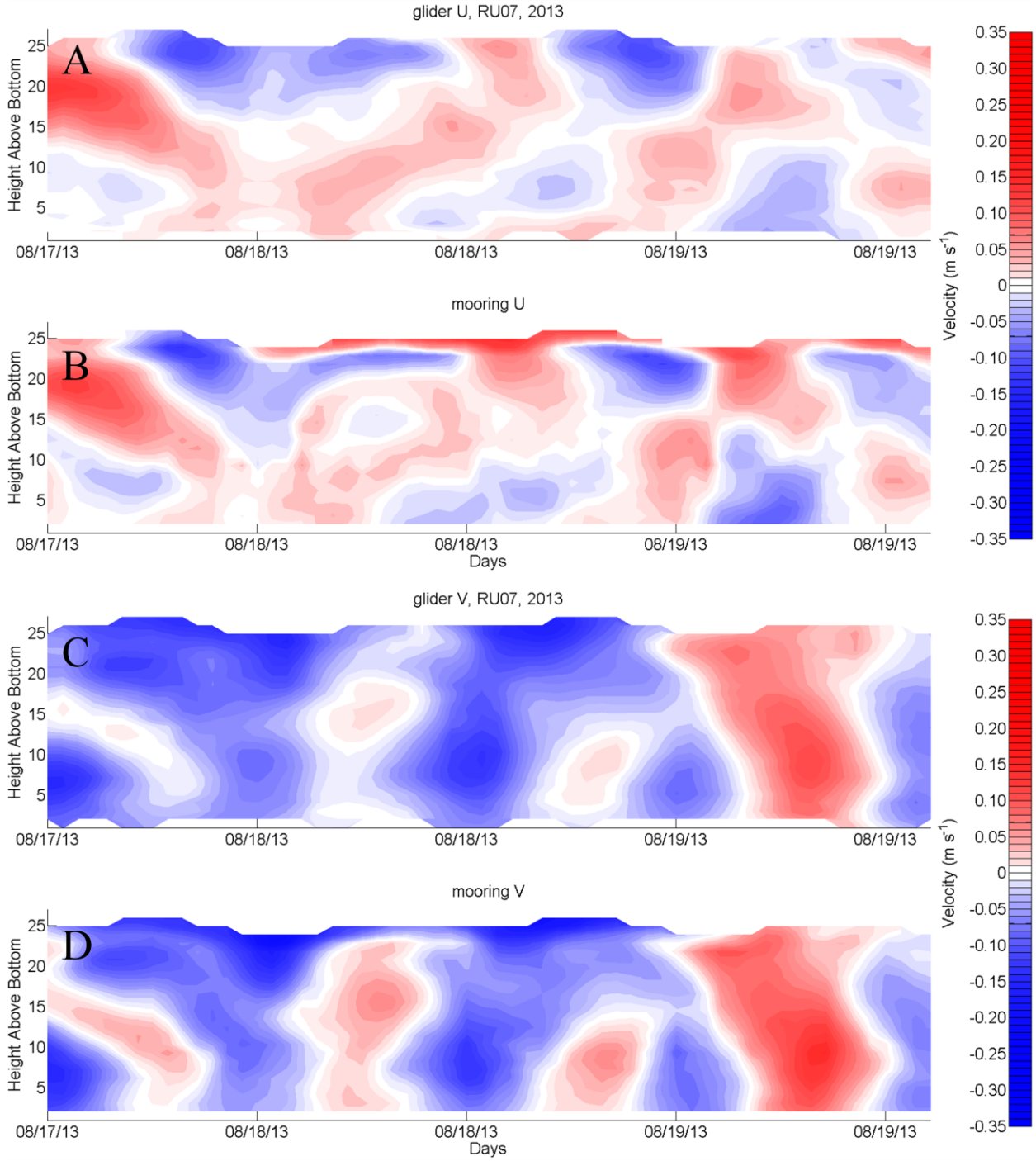

Figure 10: Contour of u(z,t) **from the glider RU07 (A) and mooring (B) and** v(z,t) **from the glider RU07 (C) and mooring (D) in 2013.** U **and** V **are positive (red) in the onshore and poleward directions, respectively.**

Figure 11

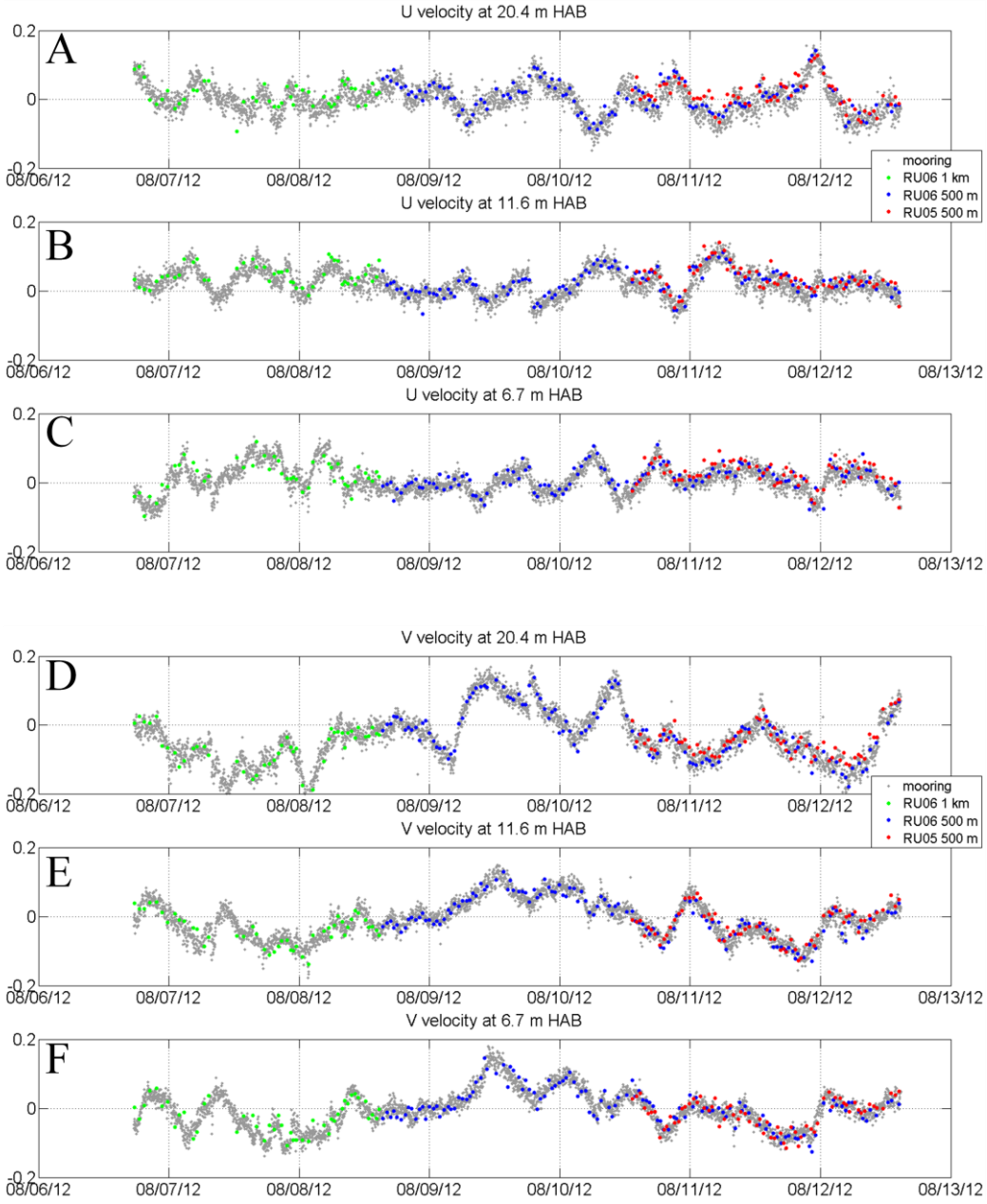

Figure 11: Time series of $u(z,t)$ **(panels A-C) and** $v(z,t)$ **(panels D-F) from the gliders in 2012. RU06 in the 1 km box (green), RU06 in the 500 m box (blue), RU05 in the 500 m box (red) and the data from the moored ADCP (gray) are shown as dots. Panels A and D are at z = 20.4 m HAB; B and E are at z = 11.6 m; C and F are at z = 6.7 m.**

Figure 12

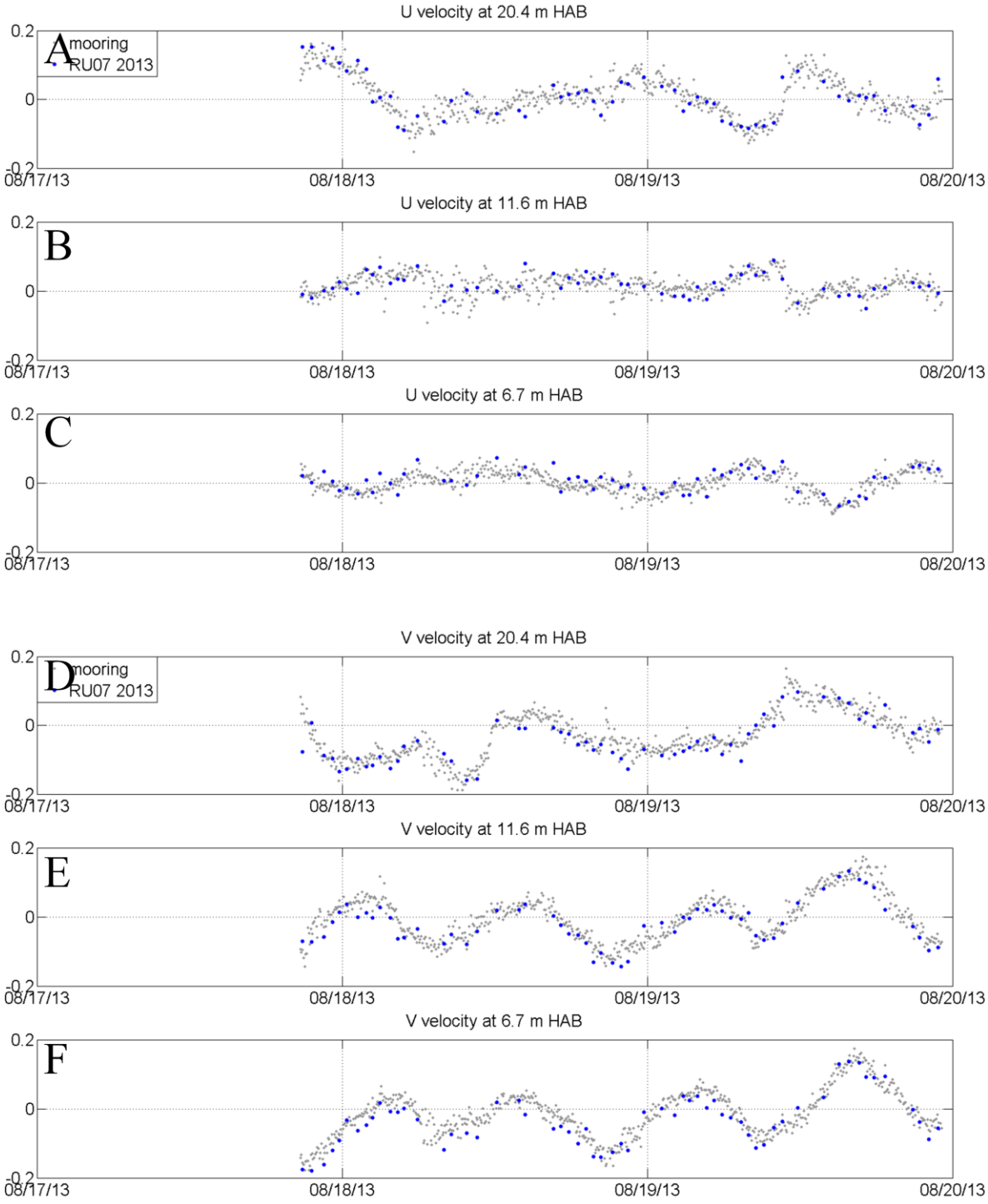

Figure 11: Time series of u(z,t) **(panels A-C) and** v(z,t) **(panels D-F) from the glider in 2013. Data from the moored ADCP (gray) and glider RU07 (blue) are shown as dots. Panels A and D are at z = 20.4 m HAB; B and E are at z = 11.6 m; C and F are at z = 6.7 m.**

Figure 13

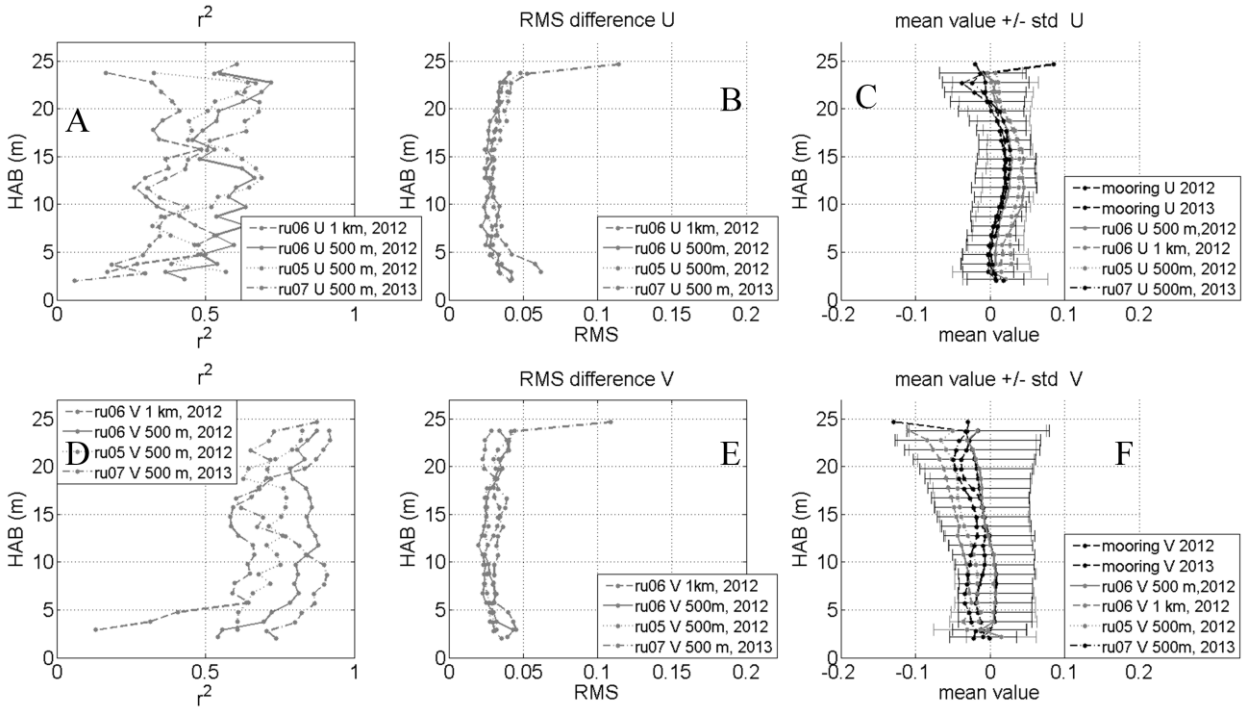

Figure 13: Vertical profiles of r^2 (A), RMS difference (B) and mean value +/- one standard deviation displayed as horizontal error bars (C) of u(z,t). Vertical profiles of r^2 (D), RMS difference (E) and mean value (F) +/- one standard deviation of v(z,t) are shown in the bottom row. Standard deviations are very similar between deployments so, for clarity, only one set of error bars for the glider and mooring are shown in C and F.

Figure 14

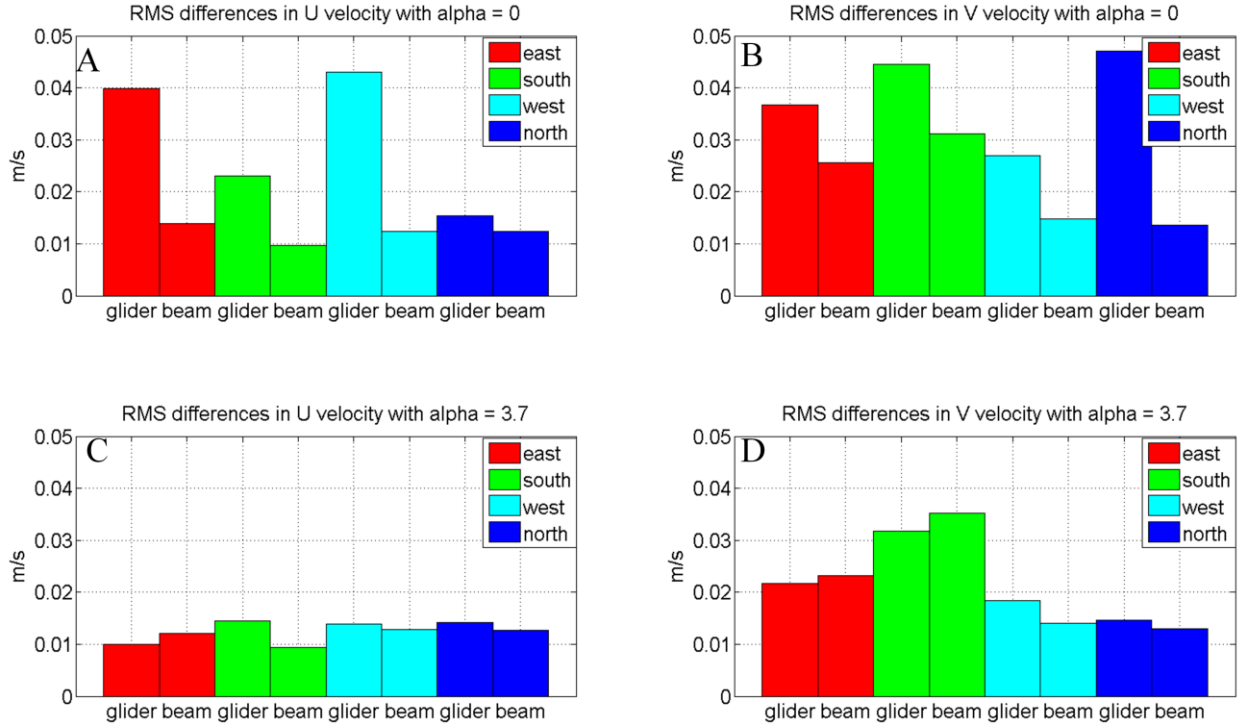

Figure 14:RMS differences between velocities measured using $U_{G,DR,GLIDER}$ and $U_{G,DR,Beam}$ and velocities measured by the bottom-mounted ADCP. Panel A and B show differences in the U and V directions, respectively with alpha = 0. Panel C and D show the effect of using alpha = 3.7.

Table 1

Glider, Box Size, Year	HAB = 20.4 m			HAB = 11.6 m			HAB = 6.7 m		
	μ_{m-g}	RMS	r^2	μ_{m-g}	RMS	r^2	μ_{m-g}	RMS	r^2
ru06, 1km, 2012	0.12	0.29	0.40	0.15	0.30	0.46	0.087	0.21	0.34
ru06, 500 m, 2012	0.057	0.22	0.69	0.083	0.16	0.62	0.05	0.09	0.47
ru05, 500 m, 2012	0.046	0.22	0.61	0.06	0.13	0.68	0.034	0.08	0.48
ru07, 500 m, 2013	-0.013	0.29	0.68	0.002	0.21	0.65	-0.027	0.13	0.42
Ru05, 500 m, 2013	-0.04	0.28	0.69	0.01	0.20	0.62	-0.30	0.12	0.48

Table 1: Mean differences of temperature measured by the glider's CTD subtracted from moored thermistors (μ_{m-g}), RMS differences, and r^2 for the three HABs in figure 3. Deployment and sampling information is noted in the far left column.